STEPS TO IMPROVING STABILITY OF THE β-PROPELLER STRUCTURE OF MYOCILIN'S OLFACTOMEDIN DOMAIN: UNDERSTANDING THE EVOLUTION OF THE β-PROPELLER

A Thesis
Presented to
The Academic Faculty

by

Michelle Sachiko Kwon

In Partial Fulfillment
of the Requirements for the Degree
Biochemistry in the
School of Chemistry and Biochemistry

Georgia Institute of Technology
May 2017

STEPS TO IMPROVING STABILITY OF THE β-PROPELLER STRUCTURE OF MYOCILIN'S OLFACTOMEDIN DOMAIN: UNDERSTANDING THE EVOLUTION OF THE β-PROPELLER

Approved by:

Dr. Raquel Lieberman, Advisor
School of Chemistry and Biochemistry
Georgia Institute of Technology

Dr. Loren Williams
School of Chemistry and Biochemistry
Georgia Institute of Technology

Date Approved: April 18, 2017

This thesis work is dedicated to:

Young Kwon
Lucy Kwon
Catherine Kwon
James Kwon

ACKNOWLEDGEMENTS

I wish to thank my principle investigator Dr. Raquel Lieberman for whom I have gained more invaluable knowledge and experience than I ever would have imagined three years ago. She has provided me with opportunities and mentorship that I will cherish and carry on with me into my future endeavors. I would also like to thank my post-doctoral advisor Dr. Shannon Hill for all her support and guidance throughout the entire research process. Dr. Hill has filled the role as my mentor and has been the greatest influence on my growth as a researcher, student, and mentor for others. I would like to thank Dr. Rebecca Donegan and Amirthaa Suntharalingam for their contributions to the project discussed in this work. I would also like to acknowledge the Petit Scholars Program for the support and funding of this project. Finally, I would like to thank all members of the Lieberman lab and my family for all their support, friendship, and love throughout my Georgia Tech undergraduate career.

TABLE OF CONTENTS

LIST OF TABLES

LIST OF FIGURES

LIST OF SYMBOLS AND ABBREVIATIONS

OLF	Olfactomedin
mOLF	Myocilin OLF domain
gOLF	Gliomedin OLF domain
D478	Aspartate 478 residue
D380	Aspartate 380 residue
N428	Asparagine 428 residue
L381	Leucine 381 residue
I477	Isoleucine 477 residue
POAG	Primary Open-Angle Glaucoma
IOP	Intraocular Pressure
TM	Trabecular Meshwork
ER	Endoplasmic Reticulum
PNS	Peripheral Nervous System
NF186	Neurofascin 186
NrCAM	Neuronal Cell Adhesion Molecules
OLFM1	Olfactomedin 1
OLFM4	Olfactomedin 4
Tm	Melting temperature
DSF	Differential Scanning Fluorimetry
MBP	Maltose-Binding Protein
WT	Wild-type
SDM	Site-Directed Mutagenesis
Sup75	Superdex 75

CD	Circular Dichroism
EIGR	Factor Xa cleavage site
PCR	Polymerase Chain Reaction
SOC	Super Optimal Broth with Catabolite Repression
AMP	Ampicillin
CAM	Chloramphenicol
LB	Luria Broth
OD	Optical Density
IPTG	isopropyl-β-D-thiogalactopyranoside
SDS-PAGE	Sodium Dodecyl Sulfate Polyacrylamide Gel Electrophoresis
SeMet	Selenomethionine
SER-CAT	Southeast Regional Collaborative Access Team
BME	2-Mercaptoethanol
Gapdh	Glyceraldehyde-3-phosphate dehydrogenase

SUMMARY

Olfactomedin (OLF) domain-containing proteins, first identified in relation to bullfrog olfactory chemoreception, are part of a superfamily of proteins implicated in many important biological functions and human diseases. The myocilin OLF domain (mOLF), one of the best studied, is closely associated with the ocular disease glaucoma. Nearly 100 myocilin mutations have been reported in glaucoma patients; >90% are missense mutations within mOLF. Disease-associated mutant myocilins are destabilized and aggregation prone, leading to toxicity and death of cells that maintain the anatomical trabecular meshwork extracellular matrix in the eye. The Lieberman lab solved the crystal structures of OLF domains from myocilin and gliomedin (gOLF), a peripheral nervous system OLF domain. While both are similar five-bladed β-propellers, only mOLF contains a stabilizing calcium ion. Remarkably, gOLF is ~20 °C more stable than mOLF, even though it doesn't have a calcium ion and is phylogenetically more primitive. The goal of this project was to use insights from mOLF and gOLF to create a thermostable mOLF. Surprisingly, mutagenesis of a calcium-coordinating aspartate (D478) to alanine abolished calcium binding but increased mOLF thermal stability to near gOLF levels. Addition of D478A to the destabilized, glaucoma-associated variant D380A rescued thermal stability to that of wild-type (WT) mOLF. Structures of thermostable mOLF variants reveal unexpected changes in tertiary structure compared to WT mOLF, which were confirmed by solution biophysical measurements. The findings from this study expand our understanding of the structure-stability relationship of mOLF and provide further insight into the evolution of the OLF β-propeller.

CHAPTER 1

INTRODUCTION

Olfactomedin (OLF) domain-containing proteins were first discovered in bullfrogs as a glycoprotein involved olfactory chemoreception[1] and are now a superfamily of proteins that have implications in important biological functions and human diseases. The best studied OLF domain-containing protein thus far is myocilin, which has been linked to the development of the ocular disease glaucoma[2], the second leading cause of blindness worldwide[3]. The modular architecture of myocilin includes an N-terminal region that contains a leucine zipper motif and two coil-coil domains and a C-terminal region that contains the OLF domain[2, 4]. More than 90% of glaucoma-associated missense mutations have been found to occur within the mOLF domain here[2, 5], highlighting the biomedical importance of understanding structure-function relationships in mOLF.

Primary open-angle glaucoma (POAG) is the most common form of glaucoma that is clinically presented as a loss of visual acuity accompanied with increased intraocular pressure (IOP)[2]. Currently, the exact cause of the elevated IOP is still unknown but the current leading pathology involves an increase in resistance of aqueous humor outflow from aggregation in the anterior of the eye within the trabecular meshwork (TM), which functions as a filter-like mechanism composed of extracellular matrix and endothelial-like cells[2]. Disease-causing nonsynonymous myocilin mutations expressed in the TM are prone to intracellular aggregation in the endoplasmic reticulum (ER), causing TM cell death, leading to reduced function of the TM fluid outflow, and, eventually, the onset of glaucoma[6].

An additional OLF domain-containing protein called gliomedin (gOLF) or collomin, has been classified as part of the most phylogenetically primitive OLF subfamily and has been found to be involved in peripheral nervous system (PNS) development[7-10]. The domain architecture of gliomedin includes a type II transmembrane domain and an extracellular region with two collagen domains and its OLF domain[9]. After gliomedin is synthesized in the ER of Schwann cells, the extracellular region is cleaved from the membrane via a RNKR-furin recognition site which then forms a trimer via the collagen domains[10-11] that allows for the OLF domain to bind the fibronectin-III-like domains of neurofascin 186 (NF186) and neuronal cell adhesion molecules (NrCAM)[10-12]. These two CAMs accumulate at heminodal clusters of peripheral neurons to recruit voltage-gated sodium channels[13] and thus lead to the formation and maintenance of the nodes of Ranvier for fast saltatory conduction in myelinated nerves[14].

Our lab has solved the crystal structures for both mOLF and gOLF which revealed similar five-bladed β-propeller structures[15-16]. The β-propeller is composed of blades, each containing a four-stranded antiparallel β-sheet, that form a circular arrangement around a central hydrophilic channel for ligand coordination or catalytic functions[17]. Propellers are most notable for their unique motifs, including the so-called molecular Velcro interactions that stabilize the N- and C- termini in the closed circular arrangement. Biologically, propellers are typically involved in protein-protein or protein-ligand interactions[18].

Structural overlay for comparison of mOLF and gOLF structures (Fig 1.1) did not immediately reveal marked differences between the two polypeptide chains; however, the central channels of the two structures contained differences in metal binding sites[16, 19]

(Fig 1.2). In mOLF, the central hydrophilic channel of its β-propeller contains a 7-coordinate, stabilizing, calcium ion that was identified prior to the structure by metal analysis[15, 19] and an apparent sodium ion adjacent to the calcium at a distance of ~3.4 Å[15]. Surprisingly, gOLF does not contain a coordinated calcium ion yet is ~20°C more stable than mOLF, and it is phylogenetically more primitive[7, 16]. In line with its high thermal stability, gOLF is also more resistant than mOLF to chemical unfolding [16].

Figure 1.1. Overlay of mOLF (light orange, PDB 4WXU) and gOLF (teal, PDB 4XAV) structures. In general, the OLF domain-containing proteins appear to have a very similar five-bladed β-propeller structure.

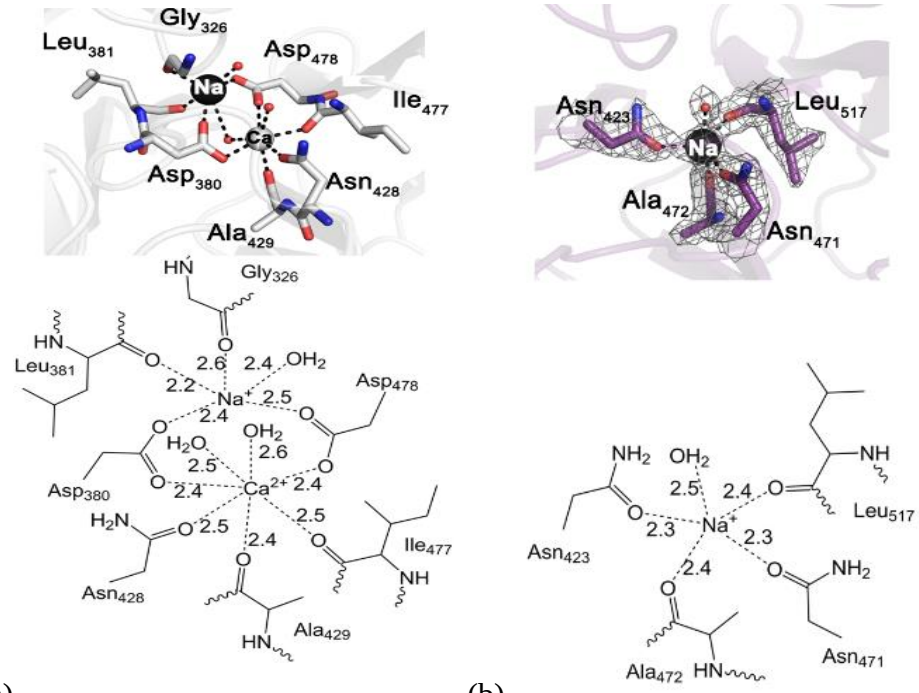

(a) (b)

Figure 1.2. Metal binding sites of (a) mOLF and (b) gOLF[16]. The hydrophobic β-propeller of mOLF contains a key calcium binding site that has been found to be implicated in thermal stability of the mOLF protein. The hydrophobic β-propeller of gOLF only contains a sodium ion in the core and does not have a novel calcium ion that is important for proper protein folding and stability. Lower panels show the interacting distances measured in Å. Reprinted by permission from PLOS ONE Publishing Group.

The surprising differences between mOLF and gOLF beg the question of why animals have mOLF in the eye where mutations, sustained UV exposure, and other environmental and mechanical stressors lead to myocilin aggregation, when a variant more similar to gOLF could, in theory, be resistant to these stressors[16]? The origin of the differing thermal stability between mOLF and gOLF appears to be due to metal binding sites located in the central cavity, which function as a tether for the blades in the β-propeller. The calcium binding site of mOLF is coordinated to the side chains of Asp380 (D380), Asn428 (N428), and Asp478 (D478) all in a monodentate fashion[15-16]. The sodium ion found in mOLF, adjacent to the calcium binding site, is coordinated by the side chains of aggregation-prone D380, D478, and Leu381 (L381)[15-16]. The D380A

variant is annotated as glaucoma-causing, destabilized from WT mOLF by ~7 °C, and calcium ion binding is abolished[15, 19]. Though variants of mOLF residue D478 have not yet been identified in populations, based on the same principles of metal ion stabilization, mutagenesis of the D478 residue was predicted to destabilize mOLF. As an alternative to cation binding, increased hydrophobic interactions, which have been suggested to also have a role in structural stability of the β-propeller[20], could also be at play in thermally stabilizing gOLF over mOLF. Indeed, when comparing hydrophobic interactions of gOLF with other OLF domains, there are 20 more hydrophobic interactions in gOLF[16].

Here we report the steps that led to thermostable variants of mOLF, based on insights on metal binding sites and nonconserved residues between gOLF, mOLF, and other related OLF domain-containing proteins. Mutagenesis of the calcium-coordinated D478 residue to a serine resulted in knockout of calcium ion binding but, surprisingly, was accompanied by an increase in mOLF thermal stability to near gOLF levels. Simultaneous mutagenesis of D478S with the disease-causing D380A variant resulted in knockout of calcium binding within the central cavity and rescued thermal stability of the mOLF variant. Structures of the thermally stable mOLF variants revealed unexpected changes in tertiary structure compared to WT mOLF, which were confirmed by solution biophysical measurements. The findings presented in this study lay the groundwork for structural-stability studies of mOLF and expand our knowledge on insight into the evolution of the OLF β-propeller.

CHAPTER 2

RATIONAL MUTAGENESIS TO INCREASE THERMAL STABILITY OF MOLF BY INCREASING HYDROPHOBICITY

Introduction

Evolutionary trace analysis across all OLF domains was conducted by Dr. Raquel Lieberman and then mapped onto the mOLF structure to assess trends in sequence conservation that could expand our knowledge on molecular characteristics among the OLF family of proteins. The evolutionary trace analysis was further analyzed by Dr. Shannon Hill for sequence differences among olfactomedin 1 (OLFM1), olfactomedin 4 (OLFM4), gOLF, and mOLF. Preliminary comparison of thermal stability, measured by melting temperature (Tm), among mOLF, OLFM4, and OLFM1 revealed that the Tm for OLFM4 is lower and that of OLFM1 is higher than mOLF[16]. Interestingly, gOLF exhibits the highest sequence divergence compared to these other OLFs, and in particular, gOLF exhibits a noticeable increase in hydrophobic amino acid residues compared to mOLF[16]. Hydrophobic interactions have been suggested to contribute significantly to the stability of the β-propeller structure[20] leading to the hypothesis that the high thermal stability associated with gOLF could be due to the more abundant hydrophobic interactions within the structure[16]. To test this hypothesis, non-glaucoma-associated single point mutations corresponding to the aligned gOLF residue were introduced into mOLF. Proteins were expressed, purified, and analyzed for an increase in Tm value via differential scanning fluorimetry (DSF).

Protein Engineering of mOLF Variants using Site-Directed Mutagenesis

Initial variants for mOLF thermal stability testing were chosen to increase hydrophobic interactions for structural stability folding of the mOLF β-propeller based on sequence alignments with gOLF. Site-directed mutagenesis (SDM) on wild type (WT) maltose-binding protein (MBP)-mOLF was conducted to obtain the following single-mutation mOLF variants: MBP-mOLF G456L, D378Y, S404A, K358L, T455L, and F307L. Mutated plasmids were confirmed by DNA sequencing aligned with WT MBP-mOLF. Point mutations are highlighted in the sequence alignments provided for each MBP-mOLF variant.

```
WTOLF       LKESPSGYLRSGEGDTGCGELVWVGEPLTLRTAETITGKYGVWMRDPKPTYPYTQETTWR
G456L       LKESPSGYLRSGEGDTGCGELVWVGEPLTLRTAETITGKYGVWMRDPKPTYPYTQETTWR
            ************************************************************

WTOLF       IDTVGTDVRQVFEYDLISQFMQGYPSKVHILPRPLESTGAVVYSGSLYFQGAESRTVIRY
G456L       IDTVGTDVRQVFEYDLISQFMQGYPSKVHILPRPLESTGAVVYSGSLYFQGAESRTVIRY
            ************************************************************

WTOLF       ELNTETVKAEKEIPGAGYHGQFPYSWGGYTDIDLAVDEAGLWVIYSTDEAKGAIVLSKLN
G456L       ELNTETVKAEKEIPGAGYHGQFPYSWGGYTDIDLAVDEAGLWVIYSTDEAKGAIVLSKLN
            ************************************************************

WTOLF       PENLELEQTWETNIRKQSVANAFIICGTLYTVSSYTSADATVNFAYDTGTGISKTLTIPF
G456L       PENLELEQTWETNIRKQSVANAFIICGTLYTVSSYTSADATVNFAYDTLTGISKTLTIPF
            ************************************************ ***********

WTOLF       KNRYKYSSMIDYNPLEKKLFAWDNLNMVTYDIKLSKM
G456L       KNRYKYSSMIDYNPLEKKLFAWDNLNMVTYDIKLSKM
            ************************************
```

Figure 2.1. DNA sequencing results for MBP-mOLF(G456L) plasmid. Raw data can be found in notebook #2 on pages 24 and 25.

```
WTOLF       LKESPSGYLRSGEGDTGCGELVWVGEPLTLRTAETITGKYGVWMRDPKPTYPYTQETTWR
D378Y       LKESPSGYLRSGEGDTGCGELVWVGEPLTLRTAETITGKYGVWMRDPKPTYPYTQETTWR
            ************************************************************

WTOLF       IDTVGTDVRQVFEYDLISQFMQGYPSKVHILPRPLESTGAVVYSGSLYFQGAESRTVIRY
D378Y       IDTVGTDVRQVFEYDLISQFMQGYPSKVHILPRPLESTGAVVYSGSLYFQGAESRTVIRY
            ************************************************************

WTOLF       ELNTETVKAEKEIPGAGYHGQFPYSWGGYTDIDLAVDEAGLWVIYSTDEAKGAIVLSKLN
D378Y       ELNTETVKAEKEIPGAGYHGQFPYSWGGYTYIDLAVDEAGLWVIYSTDEAKGAIVLSKLN
            *****************************.******************************

WTOLF       PENLELEQTWETNIRKQSVANAFIICGTLYTVSSYTSADATVNFAYDTGTGISKTLTIPF
D378Y       PENLELEQTWETNIRKQSVANAFIICGTLYTVSSYTSADATVNFAYDTGTGISKTLTIPF
            ************************************************************

WTOLF       KNRYKYSSMIDYNPLEKKLFAWDNLNMVTYDIKLSKM
D378Y       KNRYKYSSMIDYNPLEKKLFAWDNLNMVTYDIKLSKM
            ************************************
```

Figure 2.2. DNA sequencing results for MBP-mOLF(D378Y) plasmid. Raw data can be found in notebook #2 on pages 54 through 56.

```
WTOLF       LKESPSGYLRSGEGDTGCGELVWVGEPLTLRTAETITGKYGVWMRDPKPTYPYTQETTWR
S404A       LKESPSGYLRSGEGDTGCGELVWVGEPLTLRTAETITGKYGVWMRDPKPTYPYTQETTWR
            ************************************************************

WTOLF       IDTVGTDVRQVFEYDLISQFMQGYPSKVHILPRPLESTGAVVYSGSLYFQGAESRTVIRY
S404A       IDTVGTDVRQVFEYDLISQFMQGYPSKVHILPRPLESTGAVVYSGSLYFQGAESRTVIRY
            ************************************************************

WTOLF       ELNTETVKAEKEIPGAGYHGQFPYSWGGYTDIDLAVDEAGLWVIYSTDEAKGAIVLSKLN
S404A       ELNTETVKAEKEIPGAGYHGQFPYSWGGYTDIDLAVDEAGLWVIYSTDEAKGAIVLAKLN
            ************************************************************.***

WTOLF       PENLELEQTWETNIRKQSVANAFIICGTLYTVSSYTSADATVNFAYDTGTGISKTLTIPF
S404A       PENLELEQTWETNIRKQSVANAFIICGTLYTVSSYTSADATVNFAYDTGTGISKTLTIPF
            ************************************************************

WTOLF       KNRYKYSSMIDYNPLEKKLFAWDNLNMVTYDIKLSKM
S404A       KNRYKYSSMIDYNPLEKKLFAWDNLNMVTYDIKLSKM
            ************************************
```

Figure 2.3. DNA sequencing results for MBP-mOLF(S404A) plasmid. Raw data can be found in notebook #2 on pages 26 and 27.

```
WTOLF       LKESPSGYLRSGEGDTGCGELVWVGEPLTLRTAETITGKYGVWMRDPKPTYPYTQETTWR
K358L       LKESPSGYLRSGEGDTGCGELVWVGEPLTLRTAETITGKYGVWMRDPKPTYPYTQETTWR
            ************************************************************

WTOLF       IDTVGTDVRQVFEYDLISQFMQGYPSKVHILPRPLESTGAVVYSGSLYFQGAESRTVIRY
K358L       IDTVGTDVRQVFEYDLISQFMQGYPSKVHILPRPLESTGAVVYSGSLYFQGAESRTVIRY
            ************************************************************

WTOLF       ELNTETVKAEKEIPGAGYHGQFPYSWGGYTDIDLAVDEAGLWVIYSTDEAKGAIVLSKLN
K358L       ELNTETVKAELEIPGAGYHGQFPYSWGGYTDIDLAVDEAGLWVIYSTDEAKGAIVLSKLN
            **********************************************************

WTOLF       PENLELEQTWETNIRKQSVANAFIICGTLYTVSSYTSADATVNFAYDTGTGISKTLTIPF
K358L       PENLELEQTWETNIRKQSVANAFIICGTLYTVSSYTSADATVNFAYDTGTGISKTLTIPF
            ************************************************************

WTOLF       KNRYKYSSMIDYNPLEKKLFAWDNLNMVTYDIKLSKM
K358L       KNRYKYSSMIDYNPLEKKLFAWDNLNMVTYDIKLSKM
            ************************************
```

Figure 2.4. DNA sequencing results for MBP-mOLF(K358L) plasmid. Raw data can be found in notebook #2 on pages 39 and 40.

```
WTOLF       LKESPSGYLRSGEGDTGCGELVWVGEPLTLRTAETITGKYGVWMRDPKPTYPYTQETTWR
T455L       LKESPSGYLRSGEGDTGCGELVWVGEPLTLRTAETITGKYGVWMRDPKPTYPYTQETTWR
            ************************************************************

WTOLF       IDTVGTDVRQVFEYDLISQFMQGYPSKVHILPRPLESTGAVVYSGSLYFQGAESRTVIRY
T455L       IDTVGTDVRQVFEYDLISQFMQGYPSKVHILPRPLESTGAVVYSGSLYFQGAESRTVIRY
            ************************************************************

WTOLF       ELNTETVKAEKEIPGAGYHGQFPYSWGGYTDIDLAVDEAGLWVIYSTDEAKGAIVLSKLN
T455L       ELNTETVKAEKEIPGAGYHGQFPYSWGGYTDIDLAVDEAGLWVIYSTDEAKGAIVLSKLN
            ************************************************************

WTOLF       PENLELEQTWETNIRKQSVANAFIICGTLYTVSSYTSADATVNFAYDTGTGISKTLTIPF
T455L       PENLELEQTWETNIRKQSVANAFIICGTLYTVSSYTSADATVNFAYDLGTGISKTLTIPF
            ********************************************** ***************

WTOLF       KNRYKYSSMIDYNPLEKKLFAWDNLNMVTYDIKLSKM
T455L       KNRYKYSSMIDYNPLEKKLFAWDNLNMVTYDIKLSKM
            ************************************
```

Figure 2.5. DNA sequencing results for MBP-mOLF(T455L) plasmid. Raw data can be found in notebook #2 on pages 56 through 58.

```
WTOLF       LKESPSGYLRSGEGDTGCGELVWVGEPLTLRTAETITGKYGVWMRDPKPTYPYTQETTWR
F307L       LKESPSGYLRSGEGDTGCGELVWVGEPLTLRTAETITGKYGVWMRDPKPTYPYTQETTWR
            ************************************************************

WTOLF       IDTVGTDVRQVFEYDLISQFMQGYPSKVHILPRPLESTGAVVYSGSLYFQGAESRTVIRY
F307L       IDTVGTDVRQVFEYDLISQLMQGYPSKVHILPRPLESTGAVVYSGSLYFQGAESRTVIRY
            ******************.*****************************************

WTOLF       ELNTETVKAEKEIPGAGYHGQFPYSWGGYTDIDLAVDEAGLWVIYSTDEAKGAIVLSKLN
F307L       ELNTETVKAEKEIPGAGYHGQFPYSWGGYTDIDLAVDEAGLWVIYSTDEAKGAIVLSKLN
            ************************************************************

WTOLF       PENLELEQTWETNIRKQSVANAFIICGTLYTVSSYTSADATVNFAYDTGTGISKTLTIPF
F307L       PENLELEQTWETNIRKQSVANAFIICGTLYTVSSYTSADATVNFAYDTGTGISKTLTIPF
            ************************************************************

WTOLF       KNRYKYSSMIDYNPLEKKLFAWDNLNMVTYDIKLSKM
F307L       KNRYKYSSMIDYNPLEKKLFAWDNLNMVTYDIKLSKM
            ************************************
```

Figure 2.6. DNA sequencing results for MBP-mOLF(F307L) plasmid. Raw data can be found in notebook #2 on pages 109 through 112.

Purification of MBP-mOLF Variants

Growth expression yields for MBP-mOLF variants ranged between 7 g/L and 10 g/L (Table 2.1). Small scale protein purification for each variant involved lysing 3g of MBP-mOLF containing *E. coli* cell paste followed by affinity and size-exclusion chromatography. An amylose affinity column was used to isolate the fusion protein MBP-mOLF variants followed by a size exclusion polishing step using a Superdex 75 (sup75) column. Purity was assessed by sodium dodecyl sulfate polyacrylamide gel electrophoresis (SDS-PAGE) (Fig 2.8-2.9). MBP-mOLF fusion protein variants were concentrated and buffer-exchanged in the appropriate HEPES buffer for thermal stability experiments. Overlayed sup75 traces of MBP-mOLF variants are provided in Figure 2.7. The first peak in the chromatograms represents aggregated protein and the second peak consists of fusion protein with monomer and free maltose. These fusion protein variants were not further cleaved with Factor Xa to remove the MBP-tag. Purified protein yields

ranged from 0.081 mg/g cell paste for MBP-mOLF(D378Y) to 1.763 mg/g cell paste for MBP-mOLF(G456L).

Table 2.1. Growth expression yields and protein expression yields for MBP-mOLF variants.

Olfactomedin Domain	Cell Paste Yield (g/L)	Protein Yield (mg/g cell paste)
MBP-mOLF(G456L)	7.6	1.763
MBP-mOLF(D378Y)	6.8	0.081
MBP-mOLF(S404A)	7.4	0.273
MBP-mOLF(K358L)	7.9	0.488
MBP-mOLF(T455L)	11.0	0.266
MBP-mOLF(F307L)	7.0	0.932

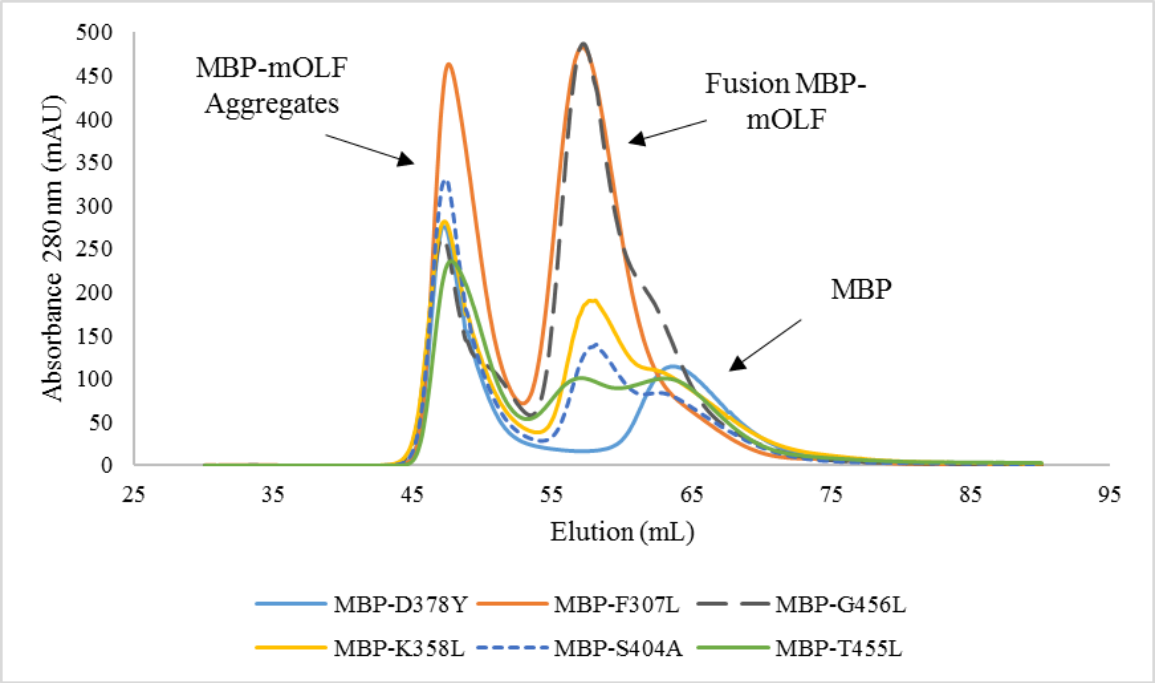

Figure 2.7. Overlay of sup75 chromatograms for fusion mOLF variants for increasing hydrophobic interactions. The first eluted peaks are MBP-mOLF aggregates and the second eluted peaks contained fusion MBP-mOLF protein.

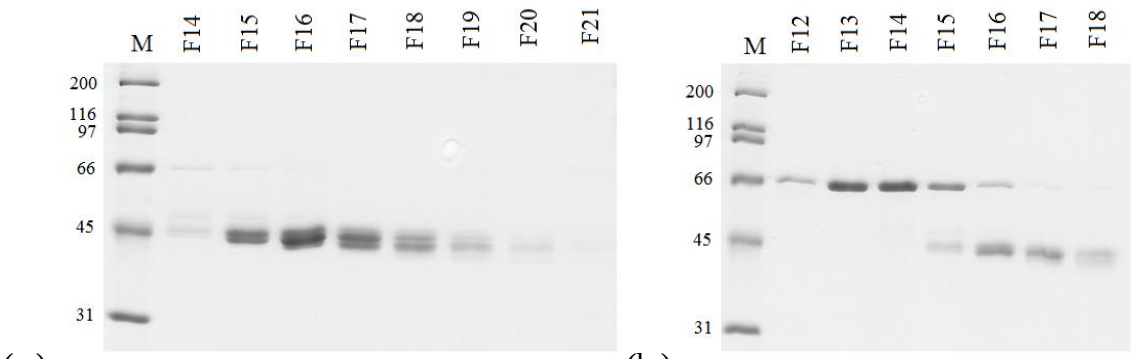

(a.) (b.)

Figure 2.8. (a.) MBP-mOLF(D378Y) and (b.) MBP-mOLF(S404A) purification assessment from size exclusion chromatography on sup75 column by 12% resolving gel. MBP is represented by the band at 45 kDa and fusion MBP-mOLF variant protein is represented by bands around 66 kDa. MBP-mOLF(D378Y) was observed to have very little fusion protein yield. Fractions 14 and 15 were used for MBP-mOLF(D378Y) thermal stability assessments. Fractions 13 and 14 were used for MBP-mOLF(S404A) thermal stability assessments.

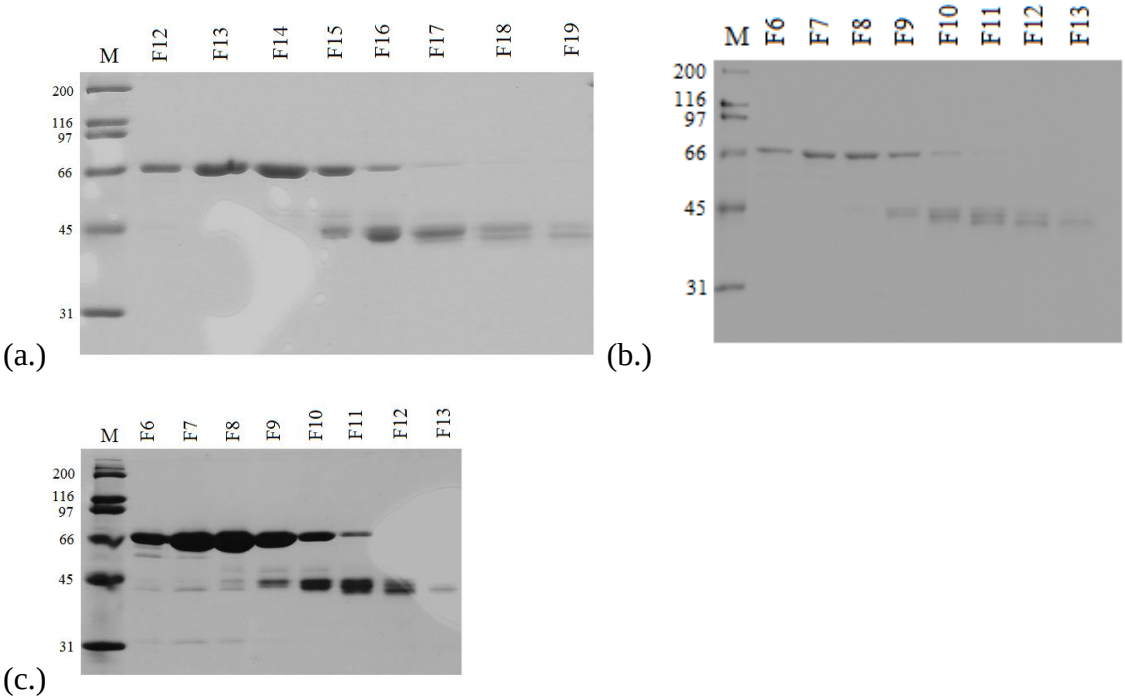

(a.) (b.)

(c.)

Figure 2.9. (a.) MBP-mOLF(K358L), (b.) MBP-mOLF(T455L), and (c.) MBP-mOLF(F307L) purification assessment from size exclusion chromatography on sup75 column by 12% resolving gel. MBP is represented by the band at 45 kDa and fusion MBP-mOLF variant protein is represented by bands around 66 kDa. Fractions 13 and 14 were used for MBP-mOLF(K358L) thermal stability assessments. Fractions 7 and 8 were used for MBP-mOLF(T455L) thermal stability testing. Fractions 7 and 8 were used for MBP-mOLF(F307L) thermal stability testing.

Thermal Stability

The six purified MBP-mOLF variants were evaluated for thermal stability via DSF. Tm values of MBP-mOLF variants were used to assess thermal stability associated with the change in hydrophobicity. All MBP-mOLF variants resulted in slight thermal destabilization except for MBP-mOLF(D378Y) resulting in severe thermal destabilization compared to WT. Decreased stabilization from MBP-mOLF(K358L) was likely due to alterations in the conformation of the B-10/C-11 loop which is thought to serve as an access gate to the central cavity of the β-propeller since the mutation occurred right before the loop[15]. Severe decrease in thermal stabilization from MBP-mOLF(D378Y) reflected the degree of destabilization associated with mOLF(K423E) when cation-π interactions were disrupted[15]. Since the analyzed mutations did not disrupt ion binding, the six MBP-mOLF variants exhibited increased thermal stabilization in the presence of calcium.

Table 2.2. Thermal stability testing of mOLF variants prior to cleavage with Factor Xa using DSF. gOLF and mOLF Tm values were measured after cleavage with Factor Xa. Mutations were chosen to increase hydrophobic interactions for increased folding stability. Tm values were not found to significantly increase the thermal stability of mOLF.

Olfactomedin Domain	**Tm (°C)**	**ΔTm + Ca^{2+}**
gOLF	69.7 ± 0.1	-0.4
mOLF	51.7 ± 0.3	+7.2
MBP-mOLF(G456L)	50.8 ± 0.1	+10.1
MBP-mOLF(D378Y)	38.6 ± 0.1	+10.1
MBP-mOLF(S404A)	48.4 ± 0.2	+9.2
MBP-mOLF(K358L)	48.3 ± 0.2	+9.6
MBP-mOLF(T455L)	47.2 ± 1.2	+7.4
MBP-mOLF(F307L)	50.3 ± 0.4	+6.0

CHAPTER 3

MUTAGENESIS OF CALCIUM BINDING SITE INCREASED THERMAL STABILITY OF mOLF

Introduction

In addition to differences in hydrophobic content discussed in Chapter 2, the β-propeller structures of gOLF and mOLF also differ in metal content. The β-propeller structure of mOLF contains a sodium and calcium ion with key amino acid residues coordinated with the metal ions (Fig 1.2a). The calcium ion in mOLF is key to the structural stability and proper folding of the protein. Coordinating amino acid residues, such as D380 and isoleucine 477 (I477), are mutated in glaucoma patients and these mutants decrease thermal stability of mOLF[19]. By comparison, there is no calcium ion present in the gOLF β-propeller (Fig 1.2b) yet gOLF is about 20°C more stable than WT mOLF. In place of calcium- and sodium- coordinating D478 in mOLF is a non-coordinating asparagine residue in gOLF. This chapter focuses effects of mutating D478 on the structure and stability of mOLF. Because of its similarity to disease-causing D380, mutation of D478 was predicted to abrogate metal binding and thus destabilize mOLF. Interestingly, the results indicate the opposite stability effect with striking structural consequences.

Mutational strategy to abolish metal binding in mOLF

Multiple sequence alignment of OLF family members reveals that the region responsible for metal binding differs somewhat across OLF domain-containing proteins. Whereas calcium ligands D380 and N428 in mOLF are largely conserved, D478 exhibits more variation across OLFs (Fig 3.1). Prior studies conducted in the Lieberman lab on

D380A, a well-studied glaucoma causing mutation, abolished Ca^{2+} binding and destabilized mOLF by ~7 °C, but no systematic mutational studies have been conducted to ascertain whether thermal stability arises due to the position of the residue rather than the specific amino acid side chain. For example, D478N is a documented glaucoma variant but the effect of this residue on mOLF stability was not known prior to this work. In addition, D478 has also not been systematically investigated, perhaps because there are no documented glaucoma mutations in this region. Notably, non-metal coordinating residues (alanine (human gOLF) and a serine (mouse gOLF)) are found in this position (Fig 3.1). We predicted that like D380A, mutation of D478 to these residues would abrogate Ca^{2+} binding to mOLF and destabilize the protein. Single point mutations (D380S, D380N, D478S, D478N, D478A, D380A/D478N, D380A/D478S) were successfully introduced into mOLF or mOLF(D380A) plasmids by SDM, expressed, purified, and biophysically characterized (See Chapter 3 for Methods and Materials).

Table 3.1. Rationale behind chosen mutagenesis for mOLF.

Mutation	**Rationale**
D380A	Well studied glaucoma-causing mutant
D380N	Glaucoma-causing mutant not yet investigated
D380S	Parallels D478
D478A	Human gOLF contains an alanine
D478N	Documented glaucoma-causing variant
D478S	Mouse gOLF contains a serine
D380A/D478N	Documented glaucoma-causing variants; complete knockout of Ca^{2+} binding
D380A/D478S	Complete knockout of Ca^{2+} binding

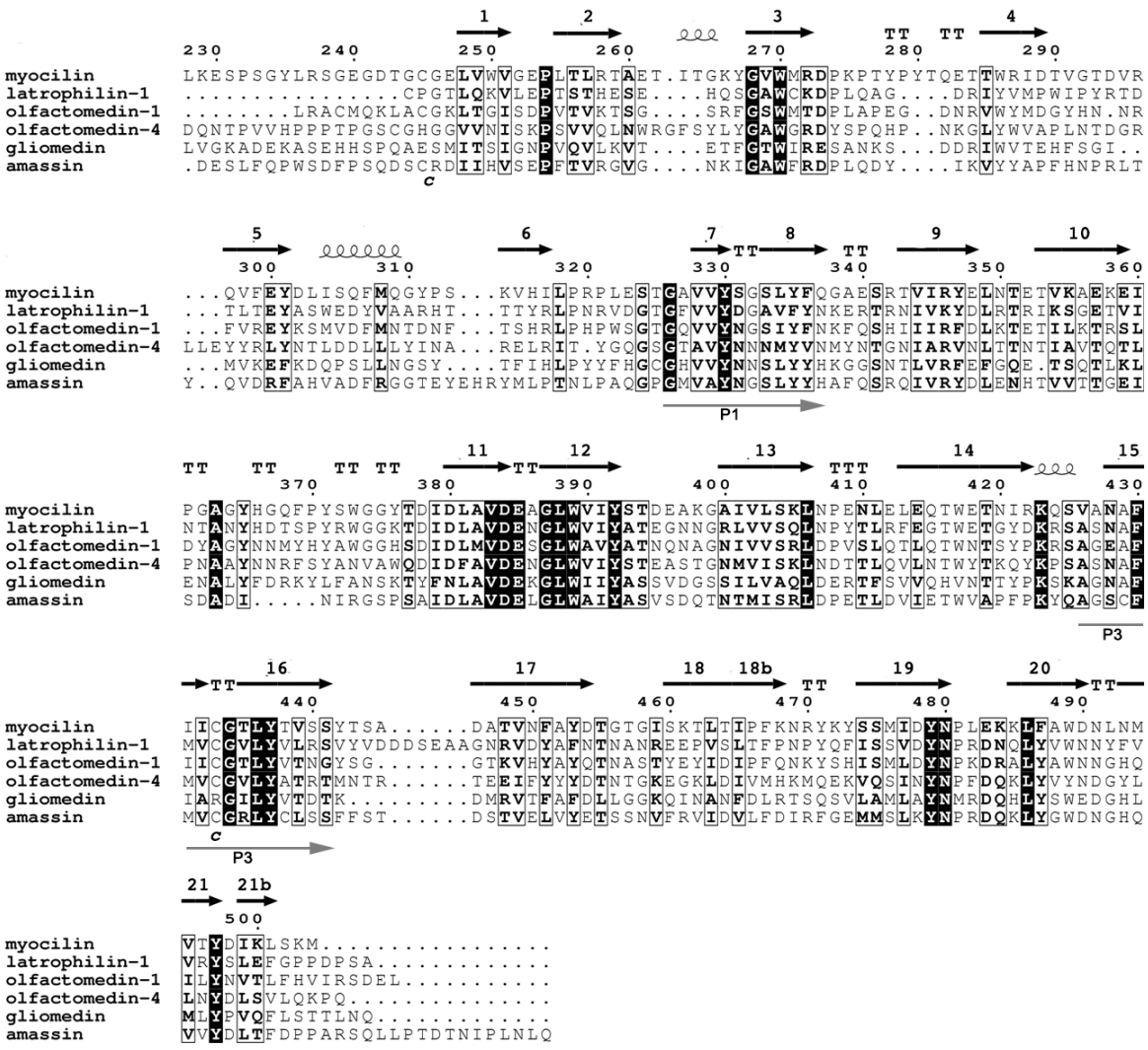

Figure 3.1. Multiple sequence alignment of OLF domain-containing proteins. Secondary structure and numbering scheme provided above alignments for mOLF. Arrows represent β-strands, helices represent α-helices, and T represents a β-turn. Reprinted by permission from Oxford University Press and Copyright Clearance Center.

```
WTOLF       LKESPSGYLRSGEGDTGCGELVWVGEPLTLRTAETITGKYGVWMRDPKPTYPYTQETTWR
D478S       LKESPSGYLRSGEGDTGCGELVWVGEPLTLRTAETITGKYGVWMRDPKPTYPYTQETTWR
            ************************************************************

WTOLF       IDTVGTDVRQVFEYDLISQFMQGYPSKVHILPRPLESTGAVVYSGSLYFQGAESRTVIRY
D478S       IDTVGTDVRQVFEYDLISQFMQGYPSKVHILPRPLESTGAVVYSGSLYFQGAESRTVIRY
            ************************************************************

WTOLF       ELNTETVKAEKEIPGAGYHGQFPYSWGGYTDIDLAVDEAGLWVIYSTDEAKGAIVLSKLN
D478S       ELNTETVKAEKEIPGAGYHGQFPYSWGGYTDIDLAVDEAGLWVIYSTDEAKGAIVLSKLN
            ************************************************************

WTOLF       PENLELEQTWETNIRKQSVANAFIICGTLYTVSSYTSADATVNFAYDTGTGISKTLTIPF
D478S       PENLELEQTWETNIRKQSVANAFIICGTLYTVSSYTSADATVNFAYDTGTGISKTLTIPF
            ************************************************************

WTOLF       KNRYKYSSMIDYNPLEKKLFAWDNLNMVTYDIKLSKM
D478S       KNRYKYSSMISYNPLEKKLFAWDNLNMVTYDIKLSKM
            **********.*************************
```

Figure 3.2. DNA sequencing results for MBP-mOLF(D478S) plasmid. Raw data can be found in notebook #1 on pages 132 through 135.

```
WTOLF       LKESPSGYLRSGEGDTGCGELVWVGEPLTLRTAETITGKYGVWMRDPKPTYPYTQETTWR
D478N       LKESPSGYLRSGEGDTGCGELVWVGEPLTLRTAETITGKYGVWMRDPKPTYPYTQETTWR
            ************************************************************

WTOLF       IDTVGTDVRQVFEYDLISQFMQGYPSKVHILPRPLESTGAVVYSGSLYFQGAESRTVIRY
D478N       IDTVGTDVRQVFEYDLISQFMQGYPSKVHILPRPLESTGAVVYSGSLYFQGAESRTVIRY
            ************************************************************

WTOLF       ELNTETVKAEKEIPGAGYHGQFPYSWGGYTDIDLAVDEAGLWVIYSTDEAKGAIVLSKLN
D478N       ELNTETVKAEKEIPGAGYHGQFPYSWGGYTDIDLAVDEAGLWVIYSTDEAKGAIVLSKLN
            ************************************************************

WTOLF       PENLELEQTWETNIRKQSVANAFIICGTLYTVSSYTSADATVNFAYDTGTGISKTLTIPF
D478N       PENLELEQTWETNIRKQSVANAFIICGTLYTVSSYTSADATVNFAYDTGTGISKTLTIPF
            ************************************************************

WTOLF       KNRYKYSSMIDYNPLEKKLFAWDNLNMVTYDIKLSKM
D478N       KNRYKYSSMINYNPLEKKLFAWDNLNMVTYDIKLSKM
            **********.*************************
```

Figure 3.3. DNA sequencing results for MBP-mOLF(D478N) plasmid. Raw data can be found in notebook #2 on pages 108 and 109.

```
WTOLF       LKESPSGYLRSGEGDTGCGELVWVGEPLTLRTAETITGKYGVWMRDPKPTYPYTQETTWR
D478A       LKESPSGYLRSGEGDTGCGELVWVGEPLTLRTAETITGKYGVWMRDPKPTYPYTQETTWR
            ************************************************************

WTOLF       IDTVGTDVRQVFEYDLISQFMQGYPSKVHILPRPLESTGAVVYSGSLYFQGAESRTVIRY
D478A       IDTVGTDVRQVFEYDLISQFMQGYPSKVHILPRPLESTGAVVYSGSLYFQGAESRTVIRY
            ************************************************************

WTOLF       ELNTETVKAEKEIPGAGYHGQFPYSWGGYTDIDLAVDEAGLWVIYSTDEAKGAIVLSKLN
D478A       ELNTETVKAEKEIPGAGYHGQFPYSWGGYTDIDLAVDEAGLWVIYSTDEAKGAIVLSKLN
            ************************************************************

WTOLF       PENLELEQTWETNIRKQSVANAFIICGTLYTVSSYTSADATVNFAYDTGTGISKTLTIPF
D478A       PENLELEQTWETNIRKQSVANAFIICGTLYTVSSYTSADATVNFAYDTGTGISKTLTIPF
            ************************************************************

WTOLF       KNRYKYSSMIDYNPLEKKLFAWDNLNMVTYDIKLSKM
D478A       KNRYKYSSMIAYNPLEKKLFAWDNLNMVTYDIKLSKM
            **********.*************************
```

Figure 3.4. DNA sequencing results for MBP-mOLF(D478A) plasmid. Raw data can be found in notebook #3 on pages 13 and 14.

```
WTOLF       LKESPSGYLRSGEGDTGCGELVWVGEPLTLRTAETITGKYGVWMRDPKPTYPYTQETTWR
D380N       LKESPSGYLRSGEGDTGCGELVWVGEPLTLRTAETITGKYGVWMRDPKPTYPYTQETTWR
            ************************************************************

WTOLF       IDTVGTDVRQVFEYDLISQFMQGYPSKVHILPRPLESTGAVVYSGSLYFQGAESRTVIRY
D380N       IDTVGTDVRQVFEYDLISQFMQGYPSKVHILPRPLESTGAVVYSGSLYFQGAESRTVIRY
            ************************************************************

WTOLF       ELNTETVKAEKEIPGAGYHGQFPYSWGGYTDIDLAVDEAGLWVIYSTDEAKGAIVLSKLN
D380N       ELNTETVKAEKEIPGAGYHGQFPYSWGGYTDINLAVDEAGLWVIYSTDEAKGAIVLSKLN
            *********************************:**************************

WTOLF       PENLELEQTWETNIRKQSVANAFIICGTLYTVSSYTSADATVNFAYDTGTGISKTLTIPF
D380N       PENLELEQTWETNIRKQSVANAFIICGTLYTVSSYTSADATVNFAYDTGTGISKTLTIPF
            ************************************************************

WTOLF       KNRYKYSSMIDYNPLEKKLFAWDNLNMVTYDIKLSKM
D380N       KNRYKYSSMIDYNPLEKKLFAWDNLNMVTYDIKLSKM
            ************************************
```

Figure 3.5. DNA sequencing results for MBP-mOLF(D380N) plasmid. Raw data can be found in Dr. Shannon Hill's notebook #14 on page 91.

```
WTOLF       LKESPSGYLRSGEGDTGCGELVWVGEPLTLRTAETITGKYGVWMRDPKPTYPYTQETTWR
D380S       LKESPSGYLRSGEGDTGCGELVWVGEPLTLRTAETITGKYGVWMRDPKPTYPYTQETTWR
            ************************************************************

WTOLF       IDTVGTDVRQVFEYDLISQFMQGYPSKVHILPRPLESTGAVVYSGSLYFQGAESRTVIRY
D380S       IDTVGTDVRQVFEYDLISQFMQGYPSKVHILPRPLESTGAVVYSGSLYFQGAESRTVIRY
            ************************************************************

WTOLF       ELNTETVKAEKEIPGAGYHGQFPYSWGGYTDIDLAVDEAGLWVIYSTDEAKGAIVLSKLN
D380S       ELNTETVKAEKEIPGAGYHGQFPYSWGGYTDISLAVDEAGLWVIYSTDEAKGAIVLSKLN
            ********************************.***************************

WTOLF       PENLELEQTWETNIRKQSVANAFIICGTLYTVSSYTSADATVNFAYDTGTGISKTLTIPF
D380S       PENLELEQTWETNIRKQSVANAFIICGTLYTVSSYTSADATVNFAYDTGTGISKTLTIPF
            ************************************************************

WTOLF       KNRYKYSSMIDYNPLEKKLFAWDNLNMVTYDIKLSKM
D380S       KNRYKYSSMIDYNPLEKKLFAWDNLNMVTYDIKLSKM
            ************************************
```

Figure 3.6. DNA sequencing results for MBP-mOLF(D380S) plasmid. Raw data can be found in Dr. Shannon Hill's notebook #14 on page 92.

```
WTOLF        LKESPSGYLRSGEGDTGCGELVWVGEPLTLRTAETITGKYGVWMRDPKPTYPYTQETTWR
D380A/       LKESPSGYLRSGEGDTGCGELVWVGEPLTLRTAETITGKYGVWMRDPKPTYPYTQETTWR
D478S        ************************************************************

WTOLF        IDTVGTDVRQVFEYDLISQFMQGYPSKVHILPRPLESTGAVVYSGSLYFQGAESRTVIRY
D380A/       IDTVGTDVRQVFEYDLISQFMQGYPSKVHILPRPLESTGAVVYSGSLYFQGAESRTVIRY
D478S        ************************************************************

WTOLF        ELNTETVKAEKEIPGAGYHGQFPYSWGGYTDIDLAVDEAGLWVIYSTDEAKGAIVLSKLN
D380A/       ELNTETVKAEKEIPGAGYHGQFPYSWGGYTDIALAVDEAGLWVIYSTDEAKGAIVLSKLN
D478S        ********************************.***************************

WTOLF        PENLELEQTWETNIRKQSVANAFIICGTLYTVSSYTSADATVNFAYDTGTGISKTLTIPF
D380A/       PENLELEQTWETNIRKQSVANAFIICGTLYTVSSYTSADATVNFAYDTGTGISKTLTIPF
D478S        ************************************************************

WTOLF        KNRYKYSSMIDYNPLEKKLFAWDNLNMVTYDIKLSKM
D380A/       KNRYKYSSMISYNPLEKKLFAWDNLNMVTYDIKLSKM
D478S        **********.*************************
```

Figure 3.7. DNA sequencing results for MBP-mOLF(D380A/D478S) plasmid. Raw data can be found in notebook #1 on pages 127 through 131.

```
WTOLF       LKESPSGYLRSGEGDTGCGELVWVGEPLTLRTAETITGKYGVWMRDPKPTYPYTQETTWR
D380A/      LKESPSGYLRSGEGDTGCGELVWVGEPLTLRTAETITGKYGVWMRDPKPTYPYTQETTWR
D478N       ************************************************************

WTOLF       IDTVGTDVRQVFEYDLISQFMQGYPSKVHILPRPLESTGAVVYSGSLYFQGAESRTVIRY
D380A/      IDTVGTDVRQVFEYDLISQFMQGYPSKVHILPRPLESTGAVVYSGSLYFQGAESRTVIRY
D478N       ************************************************************

WTOLF       ELNTETVKAEKEIPGAGYHGQFPYSWGGYTDIDLAVDEAGLWVIYSTDEAKGAIVLSKLN
D380A/      ELNTETVKAEKEIPGAGYHGQFPYSWGGYTDIALAVDEAGLWVIYSTDEAKGAIVLSKLN
D478N       *********************************************************** 

WTOLF       PENLELEQTWETNIRKQSVANAFIICGTLYTVSSYTSADATVNFAYDTGTGISKTLTIPF
D380A/      PENLELEQTWETNIRKQSVANAFIICGTLYTVSSYTSADATVNFAYDTGTGISKTLTIPF
D478N       ************************************************************

WTOLF       KNRYKYSSMIDYNPLEKKLFAWDNLNMVTYDIKLSKM
D380A/      KNRYKYSSMINYNPLEKKLFAWDNLNMVTYDIKLSKM
D478N       **********.*************************
```

Figure 3.8. DNA sequencing results for MBP-mOLF(D380A/D478N) plasmid. Raw data can be found in notebook #3 on page 12.

Purification of mOLF Variants

Growth expression yields of each mOLF variant ranged from 5.4 g/L to 13.2 g/L (Table 3.2). Protein purification for each variant was similar, and involved lysing 3-9 g of MBP-mOLF-containing *E. coli* cell paste followed by a series of affinity and size exclusion chromatography steps. First, the fusion protein MBP-mOLF variants were isolated by amylose affinity column followed size exclusion separation on a sup75 column. To remove the MBP tag, fusion proteins were subjected to overnight cleavage reactions at a 50:1 protein to Factor Xa ratio. To isolate mOLF variants, Factor Xa cleavage reaction mixtures were purified again on amylose affinity column in which the cleaved mOLF protein variants elute in the flowthrough, followed by a final polishing step by size exclusion chromatography. Purified mOLF monomer fractions were concentrated and buffer-exchanged in appropriate buffers to be used in thermal stability measurements, intrinsic fluorescence, and crystallization (see below). Figures 3.9 and 3.10 illustrate sup75 chromatograms for mOLF variants before and after Factor Xa cleavage reactions. Purified protein yields ranged from 0.156 mg/g wet cell paste for

mOLF(D480N) to 0.568 mg/g cell paste for mOLF(D478A) (Table 3.2). Purity of sup75 fractions were assessed using 12% resolving SDS-PAGE for fusion MBP-mOLF variants and 15% resolving SDS-PAGE for cleaved mOLF variants (Fig 3.11-3.17). Cleaved mOLF protein has a size around 31 kDa and MBP aggregates were resolved around 45 kDa. Relative amounts of MBP compared to purified protein were low after Factor Xa cleavage and a round of amylose affinity and sup75 size exclusion chromatography.

Table 3.2. Growth expression yields and protein expression yields for mOLF variants.

Olfactomedin Domain	Cell Paste Yield (g/L)	Protein Yield (mg/g cell paste)
mOLF(D478S)	7.4	0.318
mOLF(D478N)	5.4	0.167
mOLF(D478A)	7.8	0.568
mOLF(D380S)	6.5	0.176
mOLF(D380N)	7.1	0.156
mOLF(D380A/D478S)	6.5	0.225
mOLF(D380A/D478N)	8.1	0.509

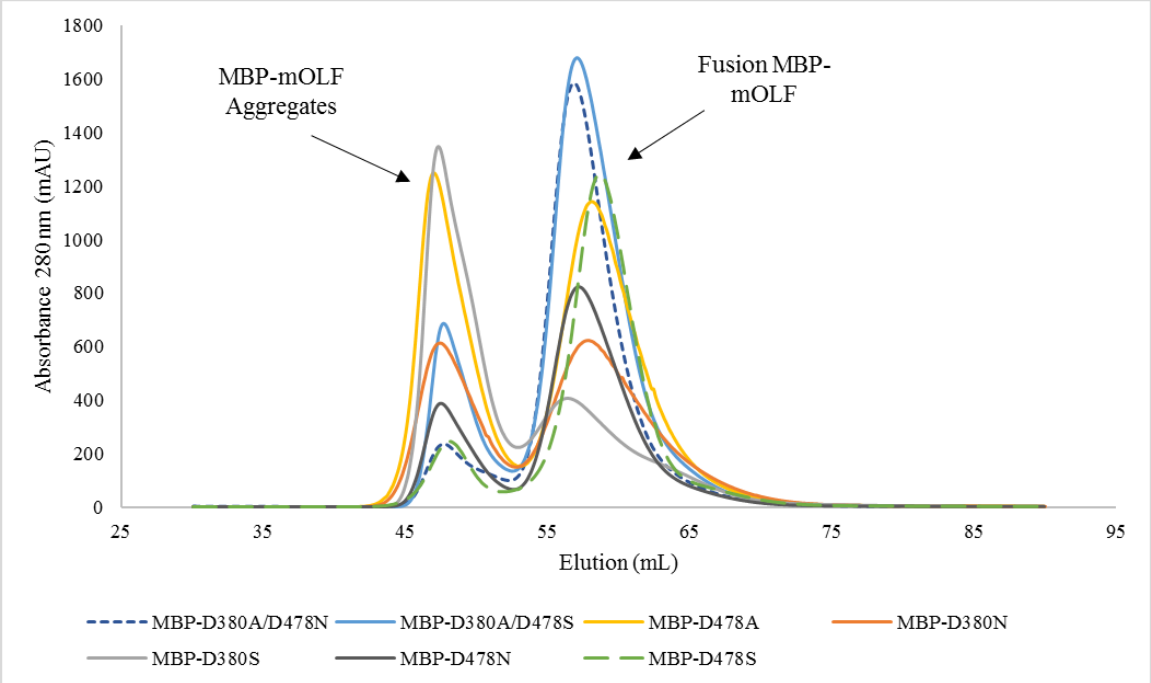

Figure 3.9. Overlay of sup75 chromatograms for fusion mOLF variants located in the calcium binding site. The first eluted peaks are MBP-mOLF aggregates and the second eluted peak contained fusion MBP-mOLF protein.

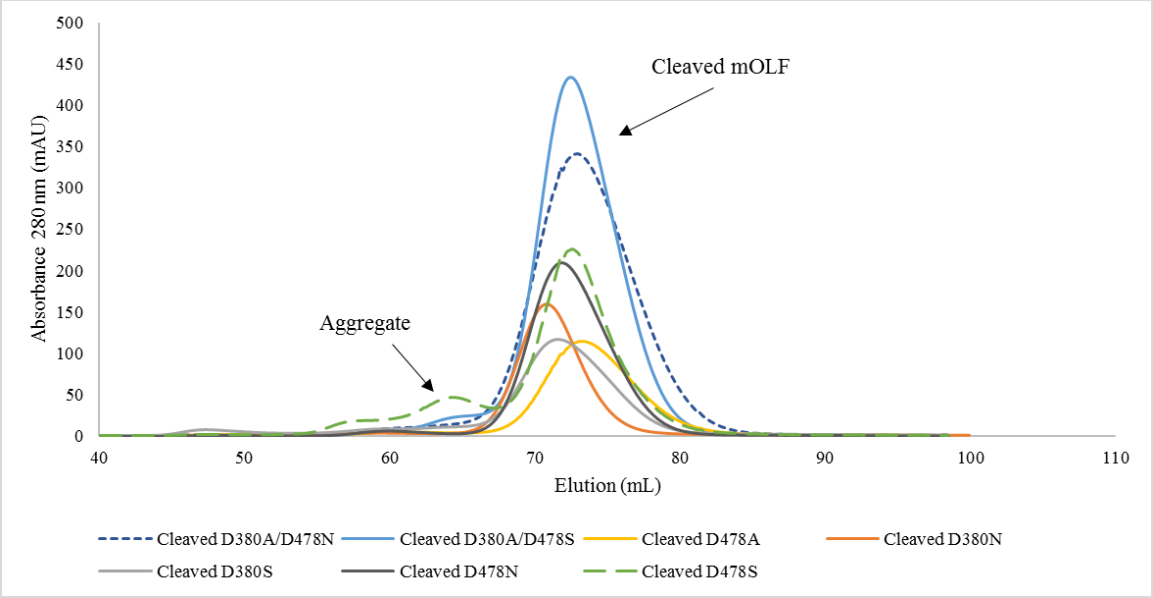

Figure 3.10. Overlay of sup75 chromatograms for cleaved mOLF variants. The first eluted peak are mOLF aggregates and the second eluted peak contained cleaved mOLF protein.

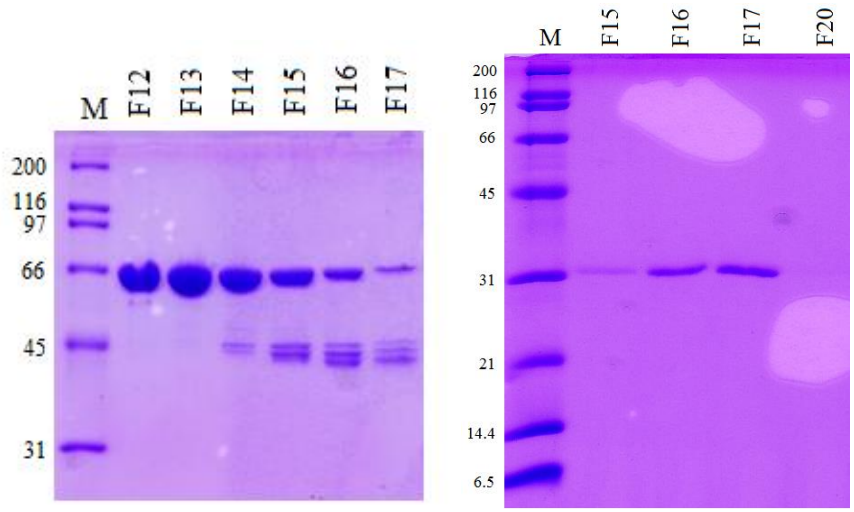

Figure 3.11. MBP-mOLF(D478S) purification assessment from size exclusion chromatography on sup75 column by 12% resolving SDS-PAGE (left). Cleaved mOLF(D478S) purification assessment from size exclusion chromatography on sup75 column by 15% resolving SDS-PAGE (right).

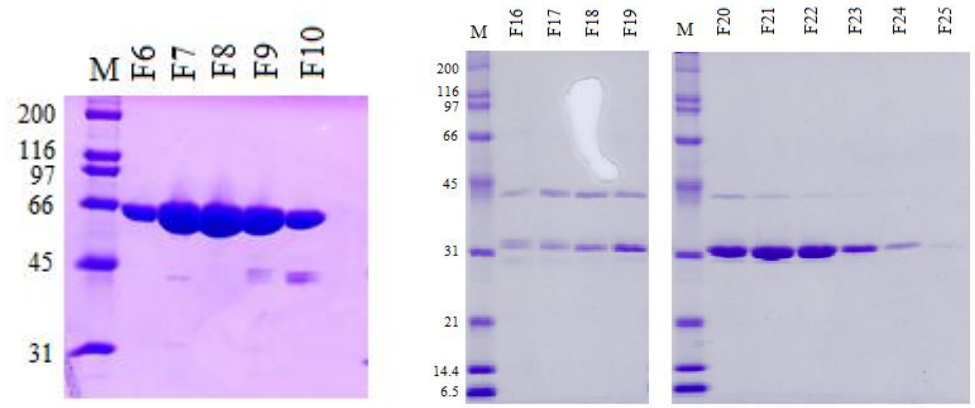

Figure 3.12. MBP-mOLF(D478N) purification assessment from size exclusion chromatography on sup75 column by 12% resolving SDS-PAGE (left). Cleaved mOLF(D478N) purification assessment from size exclusion chromatography on sup75 column by 15% resolving SDS-PAGE (right).

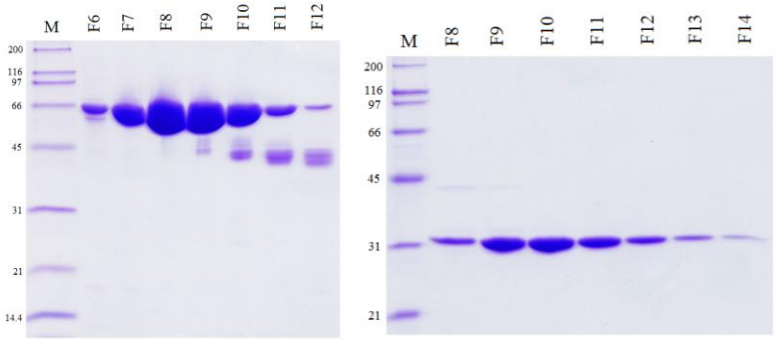

Figure 3.13. MBP-mOLF(D478A) purification assessment from size exclusion chromatography on sup75 column by 12% resolving SDS-PAGE (left). Cleaved mOLF(D478A) purification assessment from size exclusion chromatography on sup75 column by 15% resolving SDS-PAGE (right).

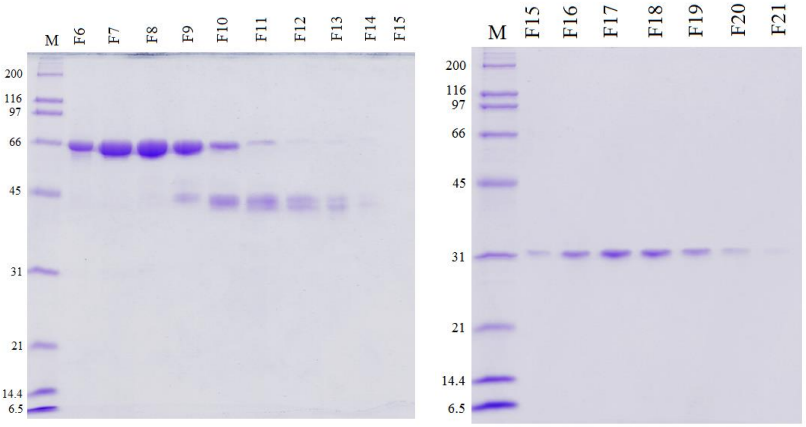

Figure 3.14. MBP-mOLF(D380S) purification assessment from size exclusion chromatography on sup75 column by 12% resolving SDS-PAGE (left). Cleaved mOLF(D380S) purification assessment from size exclusion chromatography on sup75 column by 15% resolving SDS-PAGE (right).

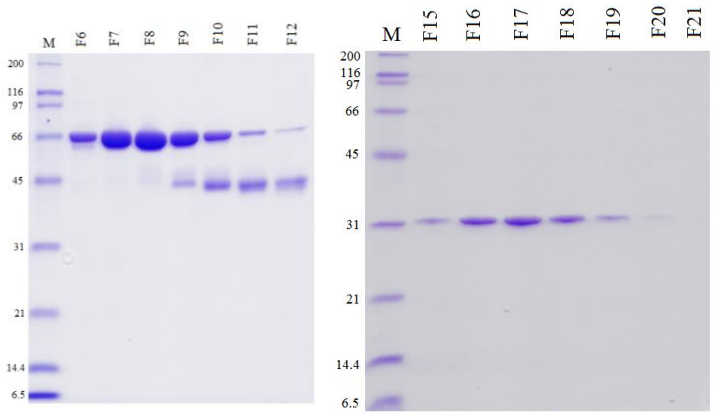

Figure 3.15. MBP-mOLF(D380N) purification assessment from size exclusion chromatography on sup75 column by 12% resolving SDS-PAGE (left). Cleaved mOLF(D380N) purification assessment from size exclusion chromatography on sup75 column by 15% resolving SDS-PAGE (right).

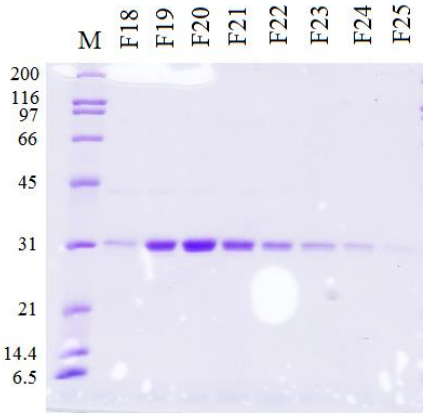

Figure 3.16. Cleaved mOLF(D380A/D478S) purification assessment from size exclusion chromatography on sup75 column by 15% resolving SDS-PAGE. Fusion protein size exclusion purification was not assessed for MBP-mOLF(D380A/D478S).

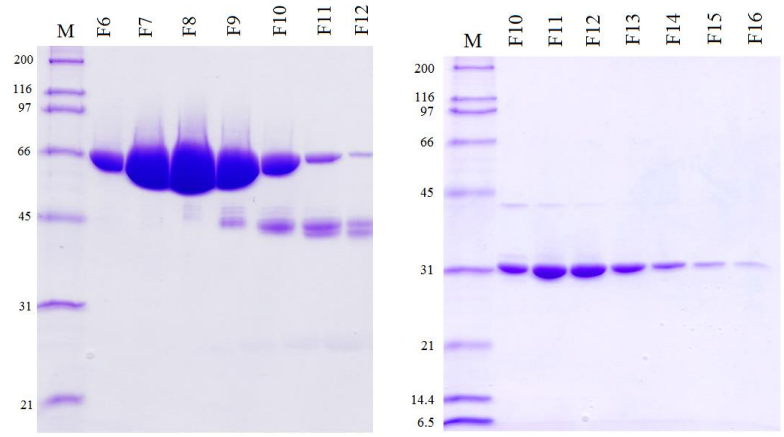

Figure 3.17. MBP-mOLF(D380A/D478N) purification assessment from size exclusion chromatography on sup75 column by 12% resolving SDS-PAGE (left). Cleaved mOLF(D380A/D478N) purification assessment from size exclusion chromatography on sup75 column by 15% resolving SDS-PAGE (right)

Thermal Stability

The seven purified, cleaved, monomeric mOLF variants were evaluated for thermal stability using DSF which uses Sypro Orange dye to monitor the increase in hydrophobicity as the protein unfolds. mOLF variants were measured in triplicate with and without 10 mM $CaCl_2$ as a convenient measure of residual calcium affinity. We expected that mOLF variants with a single point mutation at the D380 position would to be destabilizing since mOLF(D380A) is a disease-causing mutant[21] exhibiting decreased stability (Tm = 46.6°C)[19] and the D380 position is involved in coordinating the mOLF calcium ion[19]. Similarly, single point mutations at the D478 position of mOLF were also expected to be destabilizing since this residue is also involved in calcium coordination. Finally, since mutations at both D380 and D478 are expected to disrupt ion binding, the seven mOLF variants were not expected to exhibit a change in thermal stability in the presence of calcium.

Mutants at the D380 position behaved as expected, but results for mutants at D478 and the double mutants containing D380A and a mutation at D478, were

surprising. The stability of OLF(D380N) and mOLF(D380S) were both lower than that of WT mOLF (51.7 °C), comparable to the Tm for mOLF(D380A) (46.6 °C[19], and these variants were inert to the presence of calcium (Table 3.3). By contrast, mOLF(D478A), mOLF(D478N), and mOLF(D478S) exhibited ~ 5-7 °C higher stability compared to WT mOLF, though calcium binding appeared to be effectively abolished. Even more shocking was the result for double mutants mOLF(D380A/D478S), mOLF(D380A/D478N), where the increase in stability is ~10°C higher than mOLF(D380A), rescuing mOLF(D380A) to higher than WT mOLF stability. In sum, based on these experiments D380 is a position highly sensitive to destabilization concomitant with loss of calcium binding, whereas D478, and calcium binding in general, are not intrinsically destabilizing to mOLF. Moreover, D478 has the capacity to rescue the destabilizing effect imparted by D380A.

Table 3.3. Thermal stability measurements of purified, cleaved mOLF variants.

Olfactomedin Domain	**Tm (°C)**	**ΔTm + Ca^{2+}**
gOLF	69.7 ± 0.1	-0.4
mOLF	51.7 ± 0.3	+7.2
mOLF(D380A)	46.6 ± 0.3	-1.5
mOLF(D380N)	48.3 ± 0.1	+0.7
	47.9 ± 0.2	+1.3
mOLF(D380S)	45.7 ± 0.1	-0.1
	45.7 ± 0.1	-0.1
mOLF(D478A)	56.7 ± 0.1	+1.3
	57.2 ± 0.1	+1.2
mOLF(D478N)	53.8 ± 0.1	+0.4
	56.4 ± 0.1	+0.5
	56.4 ± 0.1	+0.2
	56.4 ± 0.1	+0.3
mOLF(D478S)	58.9 ± 0.1	-1.2
	58.4 ± 0.1	-0.9
mOLF(D380A/D478N)	55.2 ± 0.2	-1.5
	55.4 ± 0.1	-1.6
mOLF(D380A/D478S)	55.5 ± 0.2	-1.3
	56.5 ± 0.1	-1.5

Chemical Stability

Following thermal stability measurements, mOLF(D478S) was evaluated for chemical stability compared to WT mOLF. Unfolding and refolding trials were conducted using urea, a chaotropic agent that disrupts hydrogen bonds that are involved in tertiary structure folding. As the purified proteins become denatured, the hydrophobic interior emits at certain peak wavelengths that were detected between 300-500 nm using an excitation wavelength of 284 nm. WT mOLF and mOLF(D478S) unfolding and refolding were measured in triplicate at each different condition with 9 collections per sample. We expected mOLF(D478S) to have increased chemical stability in comparison to WT since the variant had increased thermal ability. Refolding of WT mOLF was not expected to occur since previous members of the Lieberman lab were not able to refold the protein back to native structure. Refolding of mOLF(D478S) was expected to occur since the variant was found to increase thermal stability from a single point mutation that resembled gOLF, which has been found to be capable of refolding.

Chemical stability of mOLF(D478S) was increased in comparison to WT mOLF as expected, but refolding was observed for both WT and the D478 variant. Stability of mOLF(D478S) exhibited a 0.2 M urea concentration increase for unfolding compared with WT mOLF (Fig 3.18a). Refolding of mOLF(D478S) (Fig 3.18b) appeared to be more efficient than WT mOLF refolding (Fig 3.18c) as apparent by the alignment precision of the refolded peak emission wavelengths with the peak emission wavelengths of the protein before unfolding. To sum, a single point mutation at the calcium-coordinated D478 position of mOLF was able to not only confer thermal stability of the

β-propeller structure, but it was also able to chemically stabilize the protein and more efficiently refold the denatured protein.

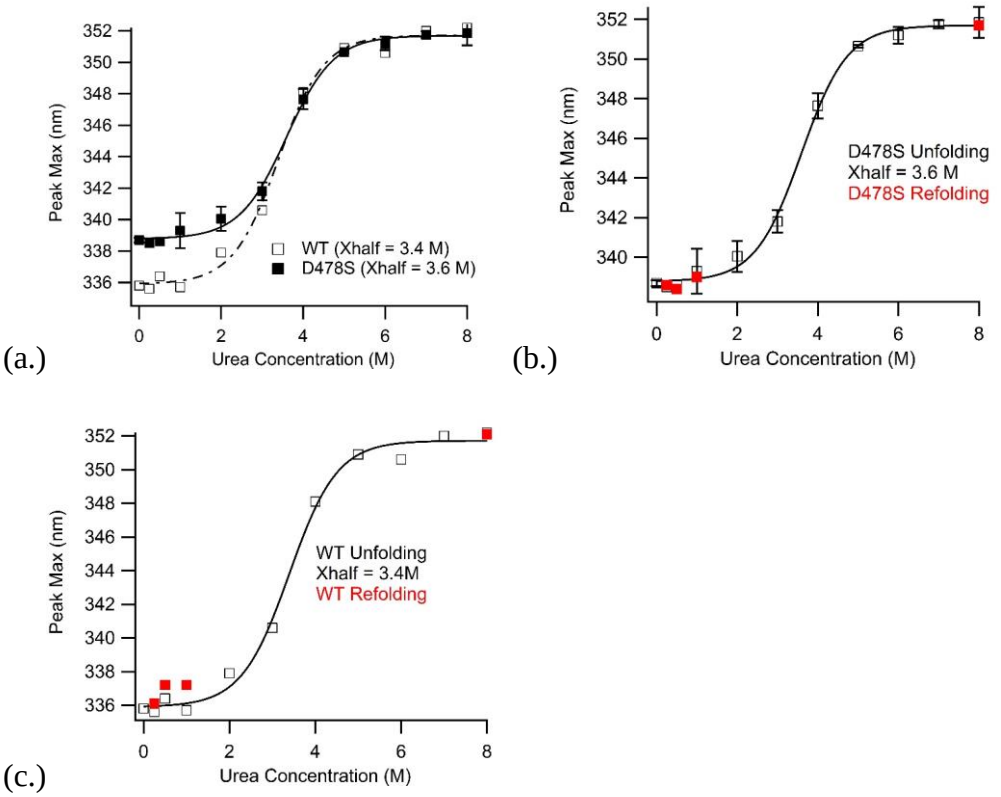

Figure 3.18. Chemical unfolding and refolding curves of WT mOLF and mOLF(D478S) using urea. (a.) Overlayed comparison of fluorescence measurements as a function of urea concentration between WT and mOLF(D478S). Refolding of (b.) mOLF(D478S) and (c.) WT mOLF are represented by the red data points.

Crystallization

We next pursued structure determination of thermally stabilizing mOLF(D478S), mOLF(D478N), and mOLF(D380A/D478S) to visualize structural changes in these variants that could account for increased stability of the mOLF β-propeller. X-ray crystallography provides a 3-D protein structure at the atomic level from diffracted beams of incident X-rays. A total of 9 optimization trays were setup for mOLF(D380A/D478S), 10 trays for mOLF(D478S), and 12 trays for mOLF(D478N). Crystal morphology resembled small “gem stones” observed under a light microscope (Fig 3.19-3.21). Crystal

structures of all three proteins were solved and refined by Dr. Shannon Hill, research scientist in the Lieberman lab.

A striking structural perturbation was revealed by all three ~ 2 Å resolution crystal structures solved by Dr. Hill. All three structures missing electron density for the helix and loops of Blade A (Fig 3.22), suggesting that these regions of the protein are not locked into a single conformation as they are in the WT structure. Thus, these structures apparently represent a partially folded state of mOLF. With a loss of helical secondary structure, this state would be expected to correspond to less, not more, stability compared to WT.

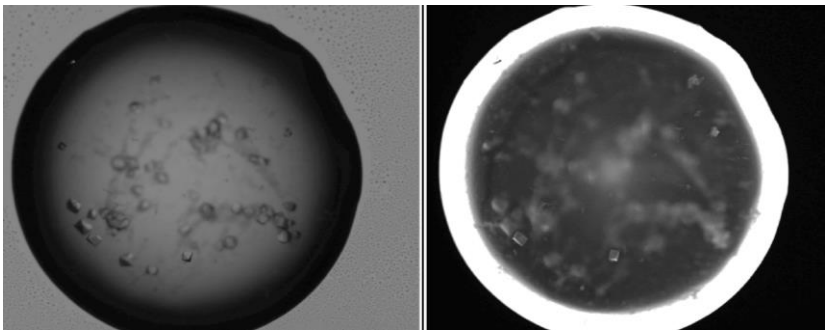

Figure 3.19. Crystal images of mOLF(D380A/D478S). Purified protein was concentrated down to 15 mg/mL and the well conditions with optimal crystal growth were 20% PEG 3350, 0.2 M BisTris, 0.2 M magnesium formate, and a 1:1 drop ratio.

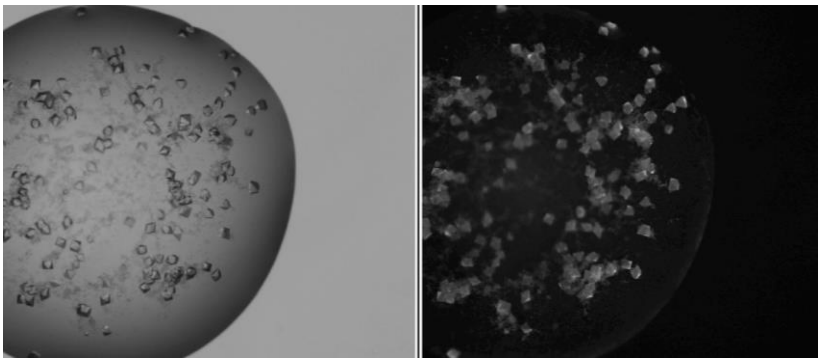

Figure 3.20. Crystal images of mOLF(D478S). Purified protein was concentrated down to 15 mg/mL and the well conditions with optimal crystal growth were 20% PEG 3350, 0.2 M BisTris, 0.2 M magnesium formate, and a 1:1 drop ratio.

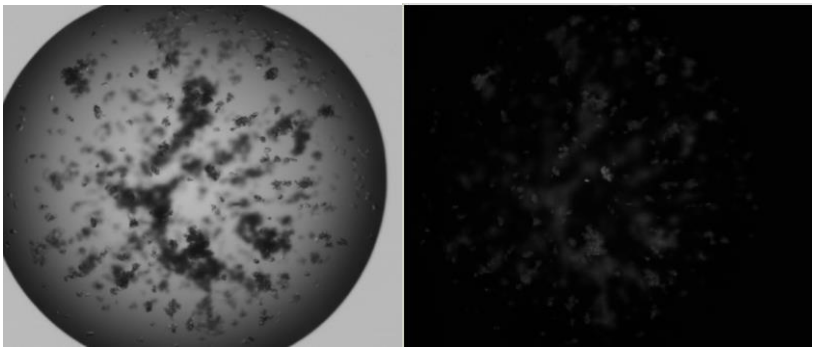

Figure 3.21. Crystal image of mOLF(D478N). Purified protein was concentrated down to 15 mg/mL and well conditions with optimal crystal growth were 20% PEG 3350, 0.2 M BisTris, 0.3 M magnesium formate, and a 1:1 drop ratio.

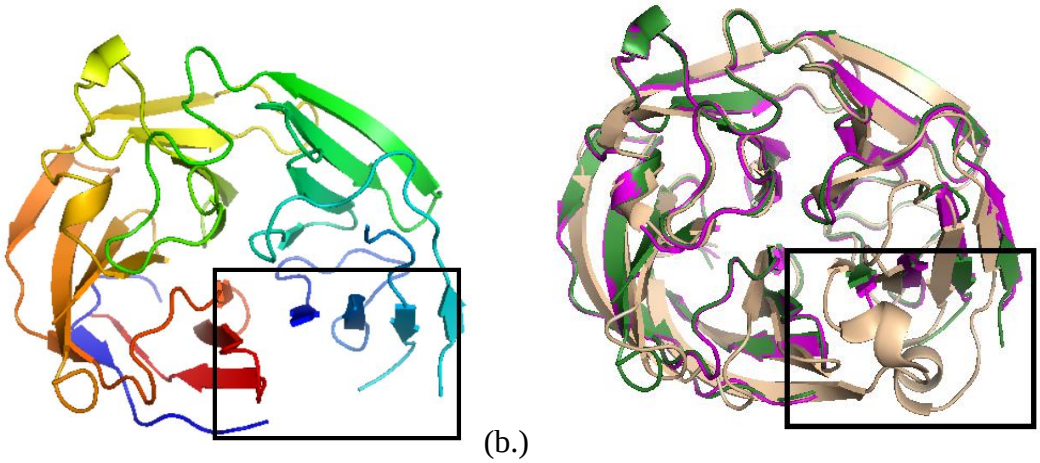

(a.) (b.)

Figure 3.22. (a.) Crystal structure of mOLF(D380A/D478S) with an Rwork of 0.2556, Rfree of 0.3169, and a resolution of 2.1 Å. Missing electron density in Blade A was consistent in all mOLF variants that contained a mutation at the D478 residue position. Missing electron density suggests that the amino acids in that region are flexible in solution. (b.) Structural overlay of WT mOLF (light pink), mOLF(D380A/D478S) (magenta), and mOLF(D478S) (green). Crystal structure of mOLF(D478S) had an Rwork of 0.1905, Rfree of 0.2308, and a resolution of 1.8 Å. Regions of missing electron density in the mOLF D478 variant structures are indicated by the boxed in areas.

Solution Structural Characterization of Stabilized mOLF Variants

To confirm the crystallographic result of apparent increased flexibility of mOLF(D478S), mOLF(D478N), and mOLF(D380A/D478S) resulting in missing electron density, near-UV circular dichroism (CD) was used to characterize and compare the tertiary structure with WT mOLF in solution. This method measures absorption of circularly polarized light by aromatic amino acid residues and serves as a readout of local

chemical environment. Phenylalanine are detected between 250-270 nm, tyrosine between 270-290 nm, and Tryptophan between 280-300 nm. In areas corresponding to missing electron density, shown in red (Fig 3.23), there are three aromatic amino acid residues, two Tyr and one Phe. Therefore, mOLF variants with increased flexibility were predicted to have deviations from WT in the Phe/Tyr region of the CD spectrum but minimal deviation in the lower energy Trp region.

CD spectra of mOLF(D478S), mOLF(D478A), mOLF(D380A/D478S), and mOLF(D380A/D478S) revealed deviations from WT mOLF spectra in the 250-290 nm range of phenylalanine and tyrosine residues (Fig 3.24), indicating non-native structures and adding further evidence that the amino acid residues missing electron density in the three crystal structures are more flexible in solution. The variant spectra are similar to CD spectra of destabilizing mOLF(D380A). Notably, the mOLF(D380A) CD spectrum had deviations from WT mOLF within the tryptophan region that appear to be corrected in the double mutant mOLF(D380A/D478S) and mOLF(D380A/D478N). These results suggest that the destabilized non-native structure imparted by D380A in mOLF can be partially rescued by a single point mutation in the D478 position.

To further confirm the crystallographic result, intrinsic fluorescence measurements were conducted on mOLF variants (Fig 3.25). This method monitors the environment of aromatic residues: when tryptophan and tyrosine residues become more surface-exposed, hydrogen bonding causes a shift to longer emission wavelengths. Based on the structures and CD spectra, we predicted a shift to longer wavelengths for the mOLF variants compared to WT. Indeed, both stabilizing mOLF mutants (D478S, D478A, D380A/D478N) and destabilizing mOLF mutants (D380N and D380S) exhibited

red-shifted fluorescence emission maxima (~338-342 nm) compared to WT mOLF (<336 nm). In sum, though it remains a mystery why some mutations are thermally stabilizing and others destabilizing, solution biophysical measurements confirm a non-native structure of mOLF variants at positions D380 and D478 in solution.

GCGELVWVGEPLTLRTAETITGK**Y**GVWMRDPKPTYPYTQETTWRIDTVGTDVRQVFEYDLIS
Q**F**MQG**Y**PSKVHILPRPLESTGAVVYSGSLYFQGAESRTVIRYELNTETVKAEKEIPGAGYHGQ
FPYSWGGYTDIDLAVDEAGLWVIYSTDEAKGAIVLSKLNPENLELEQTWETNIRKQSVANAFII
CGTLYTVSSYTSADATVNFAYDTGTGISKTLTIPFKNRYKYSSMIDYNPLEKKLFAWDNLNMV
TYDIKLSK

Figure 3.23. Amino acid sequence of mOLF. Regions of missing electron density in the D478 variant structures are indicated by the red amino acid residues. Bolded amino acid residues were the aromatic residues that are measured for changes in biophysical characterization.

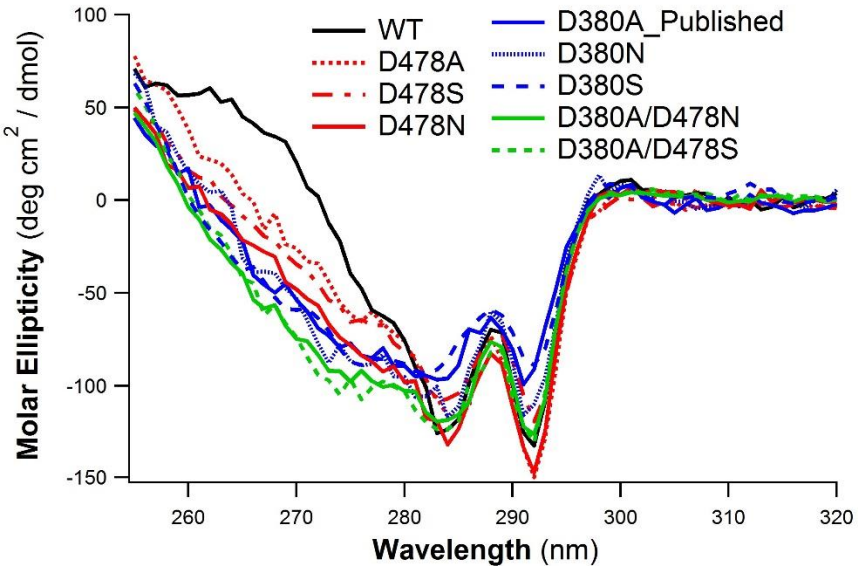

Figure 3.24. Near-UV CD spectra overlay of WT (black), mOLF(D380A) (blue solid), mOLF(D380N) (blue dotted), mOLF(D380S) (blue dash), mOLF(D478A) (red dotted), mOLF(D478S) (red dash), mOLF(D478N) (red solid), mOLF(D380A/D478N) (green solid), and mOLF(D380A/D478S) (green dash).

Point	textWave0	textWave1
0	WT	335.8 ± 0.1
1	D478A	338.3 ± 0.3
2	D478N	338.8 ± 0.2
3	D478S	338.7 ± 0.1
4	D380N	339.7 ± 0.1
5	D380S	339.7 ± 0.1
6	D380A/D478N	339.1 ± 0.1
7	D380A/D478S	339.9 ± 0.1

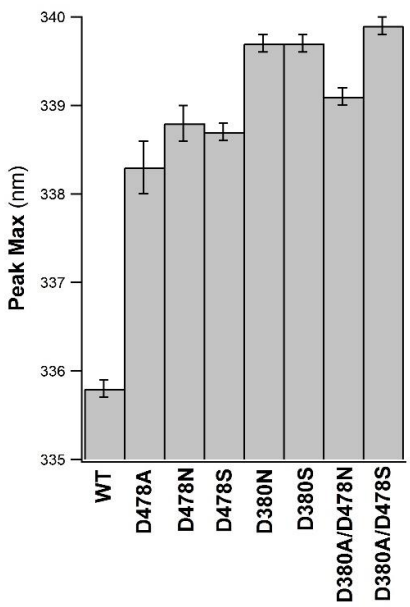

Figure 3.25. Intrinisic fluorescence measurement comparison of WT mOLF, mOLF(D478A), mOLF(D478N), mOLF(D478S), mOLF(D380N), mOLF(D380S), mOLF(D380A/D478N), and mOLF(D380A/D478S).

Cellular Secretion of Stabilizing mOLF Variants

One of the current leading molecular mechanisms for myocilin-associated glaucoma involves intracellular aggregation of misfolded myocilin disease variants, particularly within the ER, instead of secretion of myocilin to the TM in the anterior segment of the eye[22]. This aggregated protein buildup leads to ER stress, cell death[6, 15, 23]. Decreased fluid outflow from the TM is proposed to lead to accelerated increase of intraocular pressure and cause vision loss and glaucoma, particularly in children[15]. The Lieberman lab in collaboration with Chad Dickey's lab (University of South Florida) previously confirmed earlier results regarding robust secretion of WT myocilin and intracellular sequestration of disease-associated myocilin mutants in a model cell culture system[24]. The cellular behavior of the thermally stabilized, yet partially unfolded, D478 variants was not readily predicted, since the relative importance of stability and structure for cellular quality control and secretion has not been tested.

Therefore, the Dickey lab evaluated the cellular secretion profiles of WT, D380A, D478S, D478N, and D380A/D478N full-length myocilin variants, detecting extracellular (Fig 3.26) and intracellular levels of myocilin (Fig 3.27). For intracellular myocilin, analysis included solubility with and without Triton-X100, a commonly used detergent for solubilizing non-amyloid aggregates. Stabilized, non-native single point mutants, D478S and D478N on their own, and as double mutants with D380A exhibited extracellular secretion profiles similar to WT mOLF. Consistent with this result, only intracellularly-sequestered D380A were insoluble in Triton-X100. Thus, thermal stability appears to be the key parameter for proper secretion of myocilin, more so than native mOLF structure.

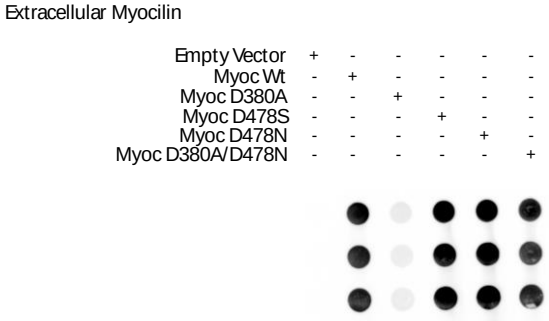

Figure 3.26. Extracellular secretion profiles of WT, D380A, D478S, D478N, and D380A/D478N myocilin. Disease-causing variant D380A is known to be prone to aggregation and lead to decreased secretion of the protein into the extracellular space.

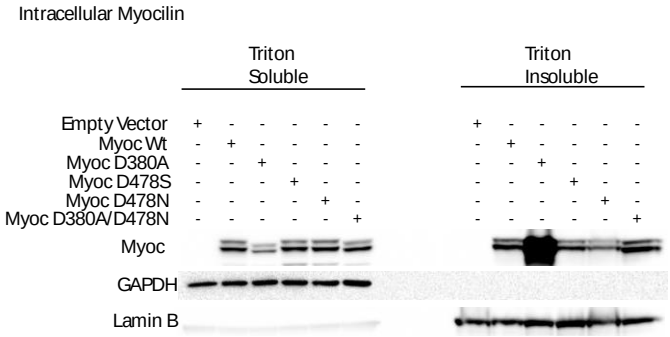

Figure 3.27. Solubility of intracellular myocilin in Triton X-100 detergent. Insoluble protein was observed only with the disease-causing D380A variant which is known to be prone to aggregation.

CHAPTER 4

EXPERIMENTAL PROCEDURES AND MATERIALS

Molecular biology

The parent WT mOLF plasmid was synthesized as previously reported[25]. Briefly, the mOLF gene corresponding to amino acid residues 228-504 of full-length human myocilin was amplified and annealed into pET-30 Xa/LIC vector (Novagen) and then subcloned into pMAL-c5x vector. The mOLF pMAL-c5x vector produces mOLF as a fusion protein with MBP which can be removed using the intervening Factor Xa cleavage site (EIGR) within the linker.

Variants of mOLF were prepared using the parent mOLF plasmid using SDM (QuikChange Lightening kit). Forward and reverse primers (Table 4.1) specific for each mOLF variant were designed using Agilent Technologies QuikChange Primer Design (http://www.genomics.agilent.com/primerDesignProgram.jsp) and purchased from MWG Operon.

Table 4.1. Forward and reverse primer designs for all mOLF variants in this study.

Mutation	Primers for Site Directed Mutagenesis
F307L	Fwd 5'-AGTATGACCTCATCAGCCAGTTAATGCAGGGCTAC-3' Rev 5'-GTAGCCCTGCATTAACTGGCTGATGAGGTCATACT-3'
K358L	Fwd 5'-GAGACAGTGAAGGCTGAGCTAGAAATCCCTGGAGCTGGC-3' Rev 5'-GCCAGCTCCAGGGATTTCTAGCTCAGCCTTCACTGTCTC-3'
D378Y	Fwd 5'-TCCACAGCCAAGTCAATATACGTGTAGCCACCCCAAG-3' Rev 5'-CTTGGGGTGGCTACACGTATATTGACTTGGCTGTGGA-3'
D380N	Fwd 5'-TGGGGTGGCTACACGGACATTAACTTGGCTGTG-3' Rev 5'-CACAGCCAAGTTAATGTCCGTGTAGCCACCCCA-3'
D380S	Fwd 5'-TGGGGTGGCTACACGGACATTAGCTTGGCTGTGGA-3' Rev 5'-TCCACAGCCAAGCTAATGTCCGTGTAGCCACCCCA-3'
S404A	Fwd 5'-CTGGGTTCAGTTTGGCGAGGACAATGGCACC-3' Rev 5'-GGTGCCATTGTCCTCGCCAAACTGAACCCAG-3'
T455L	Fwd 5'-GCTGATACCTGTGCCTAAGTCATAAGCAAAGTTGACGGTA-3' Rev 5'-TACCGTCAACTTTGCTTATGACTTAGGCACAGGTATCAGC-3'
G456L	Fwd 5'-CTTGCTGATACCTGTTAGTGTGTCATAAGCAAAGTTGACGGTAGCAT-3' Rev 5'-ATGCTACCGTCAACTTTGCTTATGACACACTAACAGGTATCAGCAAG-3'
D478A	Fwd 5'-GCAGCATGATTGCGTACAACCCCCTG-3' Rev 5'-CAGGGGGTTGTACGCAATCATGCTGC-3'
D478N	Fwd 5'-CGCTATAAGTACAGCAGCATGATTAACTACAACCCCCT-3' Rev 5'-AGGGGGTTGTAGTTAATCATGCTGCTGTACTTATAGCG-3'
D478S	Fwd 5'-CCGCTATAAGTACAGCAGCATGATTAGCTACAACCCCCTGG-3' Rev 5'-CCAGGGGGTTGTAGCTAATCATGCTGCTGTACTTATAGCGG-3'

Primers were dissolved using the appropriate amount of nuclease free water indicated by Operon to yield a final primer concentrations of 100 μM. Forward and reverse primers were subsequently diluted to 125 ng/μL in 10 μL reaction volumes. mOLF plasmids were diluted to 50 ng/μL and 10 ng/μL in 5 μL reaction volumes. The following reagents were mixed together to end up with a total reaction volume of 50 μL in a polymerase chain reaction (PCR) tube:

- dNTP (1 μL)
- 10x reaction buffer/QC L Buffer (5 μL)
- Plasmid (1 μL)
- Forward primer (1μL)
- Reverse primer (1 μL)
- QuikSolution reagent (1.5 μL)
- DMSO (1 μL)
- RNAse free H_2O (37.5 μL)
- QuikChange Lightning Enzyme (1 μL)

Each of the reactions are placed in an S1000™ Thermal Cycler (Bio-Rad) using the following parameters:

Cycles	**Temperature**	**Time**
1	95°C	2 minutes
18	95°C	20 seconds
	68°C	10 seconds
	68°C	3.5 minutes

After the reaction came to completion, 50 µL of Membrane Binding Solution containing ethanol (Promega) was added to the PCR amplification and then transferred to a SV Minicolumn-Collection Tube for 1 min incubation at room temperature. Then, the Minicolumn assembly was centrifuged at 16,000 x g for 1 minute followed by an addition of 700 µL of Membrane Wash Solution (Promega) containing ethanol. These steps were repeated with 500 µL of Membrane Wash Solution and centrifuged for 5 minutes. To allow for any residual ethanol to evaporate, the Minicolumn assembly was centrifuged for 1 minute and then transferred to a new 1.5 mL microcentrifuge tube where 50 µL of nuclease free water was added to the minicolumn, incubated at room temperature for 1 minute, and centrifuged for 1 minute.

Once all the amplification reactions were washed, 2 µL of *Dpn* I restriction enzyme was directly added to each of the reactions and incubated at 37°C for 10 minutes. A 2 µL aliquot of *Dpn* I-treated DNA was added to 45 µL of XL10-Gold ultracompetent cells and 2 µL of β-Mercaptoethanol in a chilled 14-mL BD Falcon polypropylene round-bottom tube and incubated on ice for 30 minutes. The reactions were then heat-shocked in a 42°C water bath for exactly 30 seconds and then incubated on ice for 2 minutes. Preheated aliquots of super optimal broth with catabolite repression (SOC) medium were added to each reaction tube and incubated in the 37°C shaking incubator (225-250 rpm)

for 1 hour. After incubation, approximately 250 µL of each reaction was plated onto agar plates containing 60 µg/mL ampicillin (AMP) and incubated upside down overnight in a 37°C incubator.

DNA plasmids were isolated for sequencing to confirm mutagenesis for mOLF variants via minipreparation (miniprep). A single colony from each transformation reaction was added to 20 mL of sterilized Luria Broth (LB) containing 60 µg/mL AMP added for overnight growth in a 37°C shaking incubator (220-225 rpm). Small-scale growths were then centrifuged (4500 rpm) for 20 minutes followed by resuspension of the pelleted cells into 500 µL of P1 buffer from the QIAprep® Spin Miniprep Kit 250 (Qiagen). Resuspended cells were transferred to a 2 mL microcentrifuge tube and combined with 500 µL of P2 buffer and 700 µL of N3 buffer also from the Qiagen Miniprep Kit. Reaction mixtures were centrifuged (13000 rpm) for 20 minutes followed by 1 minute spins (13000 rpm) with supernatant applied to QIAprep Spin columns. The miniprep columns were washed with 500 µL of PB buffer followed by 750 µL of PE buffer for 1 minute spins each (13000 rpm). The column was then transferred to a new microcentrifuge tube to elute the DNA with 50 µL of nuclease free water. All isolated MBP-mOLF variant plasmids were verified by DNA sequencing (MWG Operon).

Protein expression

Plasmids were transformed into Rosetta-Gami 2 (DE3) competent cells onto agar plates containing 60 µg/mL AMP plus 34 µg/mL chloramphenicol (CAM) selective LB. Plates were placed upside down in a 37°C incubator for overnight growth. Starter cultures were prepared by adding one bacterial colony of the mOLF variant to 250 mL of LB media containing selective AMP/CAM antibiotics and the solution was incubated at

37°C with shaking overnight (225-250 rpm). For large scale cultures, 25 mL of the starter culture was used to inoculate each 1L solution of Superior broth in 2L baffled flasks, and the solutions were allowed to grow at 37°C in a shaking incubator (225-250 rpm) until the cells reached an optical density (OD) of ~1.5-1.7 measured at 600 nm. A total of 3L were grown for large scale cultures. At this point, the temperature was reduced to 18°C, flasks equilibrated for 1.5 h at 18 °C at which point protein expression was induced with 500 μM isopropyl β-D-thiogalactopyranoside (IPTG). The cells continued to incubate overnight at 18ºC for 16-18 hours. The next day, the cells were harvested by centrifugation (2380g) with 10 minute spins, flash-frozen with liquid nitrogen, and stored at -80°C.

Purification of mOLF variants

Cell paste (3 g) containing MBP-mOLF variants was resuspended in 10 mL amylose wash buffer (10 mM Na_2HPO_4, 10 mM KH_2PO_4, 200 mM NaCl, 1 mM EDTA) and 1X Roche Complete Protease Inhibitor Cocktail tablets and lysed by passage through a French Press twice. Cell debris was removed by centrifugation at 161,716g at 4°C for 45 minutes to remove cell debris. The soluble fraction was loaded onto an amylose affinity column (New England Biolabs) equilibrated with amylose wash buffer, and MBP-mOLF fusion protein was eluted with amylose elution buffer (10 mM Na_2HPO_4, 10 mM KH_2PO_4, 200 mM NaCl, 1 mM EDTA, 10 mM Maltose). Final fractionation using a Superdex 75 (GE Healthcare) size-exclusion column equilibrated with gel filtration buffer (200 mM NaCl, 10 mM Na_2HPO_4, 10 mM KH_2PO_4) isolated monomeric MBP-mOLF variants. MBP-mOLF variants with protein concentrations around 20 mg/mL were then cleaved with 1 mg/mL Factor Xa in gel filtration buffer (New England Biolabs) in a

50:1 protein to Factor Xa 10 mL reaction solution for 18 hours at room temperature. Amylose affinity chromatography was then used to separate cleaved mOLF variants, which elute in the flow-through, from uncleaved MBP-mOLF and free MBP, which bind the column. The mOLF variants were further polished by a final sup75 step followed by purity assessment with a 15% resolving SDS-PAGE.

Thermal stability measurements

Each mOLF variant was tested for thermal stability via DSF[25]. Sypro Orange (Invitrogen), a dye that is known to bind to the hydrophobic regions of proteins, was supplied as 5000 X solution in dimethylsulfoxide and was diluted in water (1:100) prior to preparation of the samples. Purified mOLFs were buffer exchanged into 10 mM HEPES pH 7.5 and 200 mM NaCl by concentrating and diluting three times using an Amicon MWCO 10K filtration device. Reactions mixtures (30 μL) containing 3 μL of diluted Sypro Orange and a final protein concentration of 3 μM were prepared in triplicate at room temperature with or without 10 mM $CaCl_2$. Samples were placed in a 96-well optical plate (Applied Biosystems) and sealed with optical film. Fluorescence measurements from DSF were obtained on Applied Biosciences Step-One Plus real time (RT)-PCR instrument to conduct a slow melt. Melts were conducted from 25 – 95 °C with a 1 °C per minute increase. Data was analyzed using OriginLab Corporation software. The Tm was calculated at the midpoint of unfolding using a Boltzmann sigmoid equation. Reported values are an average of two independent experiments.

Chemical unfolding experiments

WT and mOLF(D478S) chemical stability measurements were compared by unfolding both proteins using the chaotropic agent urea. Urea works to disrupt hydrogen

bonds that contribute to the folding of the tertiary structure to promote denaturation of the protein and expose the hydrophobic interior of the protein that emit at certain wavelengths. Stocks of 9 M urea, 10 μM purified protein, and a 10 mM Na/K phosphate pH 7.2, 0.2 M NaCl buffer were used to make the following samples:

Concentration of Urea (M)	**Concentration of Protein (μM)**	**Volume of 9M Urea (μL)**	**Volume of Buffer (μL)**	**Volume of Protein (μL)**
0	1	0	90	10
0.25	1	2.8	87.2	10
0.5	1	5.6	84.4	10
1	1	11.1	78.9	10
2	1	22.2	67.8	10
3	1	33.3	56.7	10
4	1	44.4	45.6	10
5	1	55.5	34.5	10
6	1	66.6	23.4	10
7	1	77.8	12.2	10
8	1	88.9	1.1	10

Each sample condition was prepared in triplicate and were placed in 4°C for at least 1 hour prior to measurement. All samples were measured on a Shimadzu RF-5301PC spectrofluorophotometer at an excitation wavelength of 284 nm, an emission wavelength range of 300 to 500 nm, 5 nm slit-widths on excitation and emission monochromators with 0.2 nm data intervals for 9 data collections.

Intrinsic fluorescence measurements

Purified mOLFs (WT, D380A, D380N, D380S, D478A, D478N, D478S, D380A/D478N, and D380A/D478S) were concentrated in 10 mM Na/K phosphate pH 7.2, 0.2 M NaCl buffer to compare the intrinsic fluorescence of surface exposed amino acid residues. A 1 μM sample of each purified mOLF variant was measured on a Shimadzu RF-5301PC spectrofluorophotometer at an excitation wavelength of 284 nm,

an emission wavelength range of 300 to 500 nm, 5 nm slit-widths on excitation and emission monochromators with 0.2 nm data intervals for 9 data collections. Each variant was measured in triplicate. Reported values are an average of two independent experiments.

Circular dichroism

Near-UV CD measurements were acquired on a Jasco J-815 spectropolarimeter equipped with a Jasco PTC-4245/15 temperature control system. mOLF samples at a concentration range between 1.0 - 3.5 mg/mL were measured in 10 mM Na/K phosphate pH 7.2, 0.2 M NaCl buffer at 4 ° C. Scans were measured from 250 nm to 320 nm at a rate of 50 nm/min and a data pitch of 1 nm using a 0.1 cm cuvette. Each measurement was an average of 20 scans. Data were blank-subtracted and converted to mean residue ellipticity $\Theta = Mres \times \Theta obs / 10 \times d \times c$, where Mres=112.9 is the mean residue mass calculated from the protein sequence; Θobs is the observed ellipticity (degrees) at wavelength λ; d is the pathlength (cm); and c is the protein concentration (g/ml). The reported spectra are an average of two independent measurements.

Crystallization of mOLF(D478S), mOLF(D478N), and mOLF(D380A/D478S)

Crystallization of mOLF(D478S), mOLF(D478N), and mOLF(D380A/D478S) concentrated to 15 mg/mL in 10 mM Hepes pH 7.5 were optimized from the condition used to crystallize purified selenomethionine (SeMet)-substituted mOLF E396D[15]. Crystals were grown by hanging drop method at room temperature with a 1:1 drop ratio of well solution to protein. mOLF(D478S) crystals and mOLF(D380A/D478S) crystals were grown in 20% PEG 3350, 0.2M BisTris, 0.2 M magnesium formate and were cryprotected in 20% PEG 3350, 0.2M BisTris, 0.2 M magnesium formate, 20% glycerol.

mOLF(D478N) crystals were grown in 20% PEG 3350, 0.2 M BisTris, 0.3 M magnesium formate and were cryoprotected in 15% PEG 3350, 0.1 M BisTris, 0.1 M magnesium formate, 25% glycerol. Diffraction data were collected at the Southeast Regional Collaborative Access Team (SER-CAT) 22-ID beamline and processed using HKL-2000[26]. The D380A/D478S structure was solved by molecular replacement using Phaser[27] with the myocilin olfactomedin domain E396D crystal structure (PDB code 4WXS) as the search model, followed by Phenix Auto build[28]. The mOLF(D478S) and mOLF(D478N) structures were solved by molecular replacement using the refined mOLF(D380A/D478S) structure as the search model in Phaser. The models were iteratively built and refined using Coot[29] and Phenix.refine[30].

Cellular secretion of stabilizing mOLF variants

HEK 293T cells were grown and maintained in Dulbecco's modified Eagle's Medium supplemented with 10% FBS (Sigma), 1% Sodium Pyruvate (Corning) and 1% GlutaMAX (Invitrogen) at 37°C under 5% CO_2. 6.5 * 10^5 cells/well were plated 24 hours prior to DNA transfection. Plasmid transfections were carried out in serum-free opti-mem (Invitrogen) medium via lipofection. 1µg: 2.5 µl ratio of Plasmid: Lipofectamine 2000 was used. Cells were transfected for 48 hours prior to harvest. The cells were harvested in Mammalian Protein Extraction Reagent (M-PER) buffer (Pierce) containing 1× protease inhibitor mixture (Calbiochem), 100 mM phenylmethylsulfonyl fluoride, and 1× phosphatase inhibitor II and III mixtures (Sigma).

Equal amounts of protein from cell lysates were prepared with 2× Laemmli sample buffer (Bio-Rad) with 2-Mercaptoethanol (BME) and denatured by boiling for 5 min at 100°C. Prepared lysates were then loaded onto a 10% Tris–glycine SDS-PAGE.

Gels were transferred onto PVDF membranes (Millipore) and blocked for 1 h at room temperature with 7% milk. Media from cells were collected and spun at 10,000g for 10 min. 200µl from each sample was added into each well of the dot blot apparatus and suctioned onto a nitrocellulose membrane. The membrane was then washed with PBS (filtered) twice and placed on Ponceau S. The membrane was blocked with 7% milk. Myocilin poly-clonal antibody was a gift from Dr. Stamer (Duke, North Carolina). Glyceraldehyde-3-phosphate dehydrogenase (Gapdh) antibody was purchased from Meridian Life Science (Saco, ME, USA). Actin antibody was purchased from Sigma. Secondary antibodies were all HRP-linked and purchased from Southern Biotechnolofies (Birmingham, AL, USA). All antibodies were added to blots in a 1:3000 dilution in 7% milk. Cellular secretion studies were completed by Amirthaa Suntharalingam from Chad Dickey's lab (University of South Florida).

CHAPTER 5

CONCLUSIONS AND FUTURE DIRECTIONS FOR A THERMOSTABLE OLFACTOMEDIN DOMAIN OF MYOCILIN

The newly available structures of closely related OLF domain-containing proteins have given us clues into the molecular details of disease involvement as well as the evolution of the β-propeller structure of OLF domains[15-16]. Sequence divergence across surface residues of OLF domains suggests that these proteins have unique binding partners and, therefore, distinct functions[16]. By contrast, sequence conservation in the internal region is much higher across the domain family, leading to the prediction that OLF proteins should have similar biophysical properties. Yet, the more phylogenetically primitive gOLF lacks a calcium binding site common among OLF domain family members and is significantly more stable than mOLF.

In line with previous efforts on engineering β-propeller structures that stressed the importance of hydrophobic interactions in the context of structural stability and proper protein folding[20], we first tested the hypothesis that increased hydrophobic interactions in gOLF confer its high thermal stability. Efforts to increase the thermal stability of the mOLF β-propeller by increasing hydrophobic interactions using residues similar to gOLF were met with lower thermal stability. It is possible that single point mutations in mOLF to residues in gOLF are insufficient to increase the global hydrophobic interactions needed to increase thermal stability. Additional studies will be needed to examine the additive effect of multiple simultaneous mutations on the overall hydrophobicity and thus stability of mOLF.

Remarkably, we discovered that mutations at a single position in mOLF, D478, result in a more stable protein that has lost the capability to bind calcium, yet exhibited new unstructured regions in mOLF. When the calcium ligand D478 was mutated to the corresponding residue in gOLF, thermal stability and resistance to chemical unfolding were increased. This result is in stark contrast to the nearly 40 other point mutations introduced into mOLF by the Lieberman lab which either had no effect on stability or were destabilizing, a hallmark of disease variants[16, 19, 25]. The combination of the mOLF(D478S) mutation with a disease-causing, destabilized variant mOLF(D380A) resulted in near WT stability and rescued secretion in a cell culture model, even though the molecular structure was not native. An interesting next step would be to test whether the effect is specific to the residue D380 or if the mOLF(D478S) variant can rescue the stability of other known disease-causing mOLF mutations.

Since the identification of distinct metal binding sites in the β-propeller central cavity of mOLF and gOLF[16], the role of these ions in stability of the β-propeller structures has been of intrigue with respect to the function and evolution of the OLF β-propeller. As previously demonstrated in our lab, the disease-causing mOLF(D380A) variant is a moderately unstable protein with non-native tertiary structure that is prone to forming fibrils[31]. Thus, calcium provides a more stabilizing role in the propeller that affects the morphology and electrostatics that are involved in intermolecular interactions[31], and perhaps helping the protein resist biomechanical stressors in the TM[19]. However, our findings in this study with mutants at position D478 in mOLF pose an interesting observation that the calcium ion is not necessary for proper folding of the

domain. A next step in this study would be probe additional sites on mOLF that allow mOLF to be converted to a protein of gOLF stability but with WT structure.

The cumulative results of this study suggest that during evolution the calcium binding site was introduced at the cost of thermal stability. In the case of mOLF, the resulting protein in the eye is highly aggregation prone and causes glaucoma. Could the calcium binding in the cavity of mOLF be an evolutionary tradeoff for an acquired functional role in signaling, e.g. for cell-cell communication[32]? If this is the case, knockout of the calcium binding site with D478S in myocilin might disrupt downstream responses to calcium ion flux. Future work probing the effects of myocilin(D478S) in cell culture and model organisms may at last unlock the still-mysterious biological function of myocilin.

REFERENCES

1. Snyder, D. A.; Rivers, A. M.; Yokoe, H.; Menco, B. P.; Anholt, R. R., Olfactomedin: Purification, characterization, and localization of a novel olfactory glycoprotein. *Biochemistry* **1991,** *30* (38), 9143-9153.

2. Resch, Z. T.; Fautsch, M. P., Glaucoma-associated myocilin: a better understanding but much more to learn. *Exp Eye Res* **2009,** *88* (4), 704-12.

3. Quigley, H. A.; Broman, A. T., The number of people with glaucoma worldwide in 2010 and 2020. *Br J Ophthalmol* **2006,** *90* (3), 262-7.

4. Kubota, R.; Noda, S.; Wang, Y.; Minoshima, S.; Asakawa, S.; Kudoh, J.; Mashima, Y.; Oguchi, Y.; Shimizu, N., A novel myosin-like protein (myocilin) expressed in the connecting cilium of the photoreceptor: molecular cloning, tissue expression, and chromosomal mapping. *Genomics* **1997,** *41*, 360-369.

5. Fingert, J. H.; Heon, E.; Liebmann, J. M.; Yamamoto, T.; Craig, J. E.; Rait, J.; Kawase, K.; Hoh, S. T.; Buys, Y. M.; Dickinson, J.; Hockey, R. R.; Williams-Lyn, D.; Trope, G.; Kitazawa, Y.; Ritch, R.; Mackey, D. A.; Alward, W. L.; Sheffield, V. C.; Stone, E. M., Analysis of myocilin mutations in 1703 glaucoma patients from five different populations. *Human Molecular Genetics* **1999,** *8* (5), 899-905.

6. Liu, Y.; Vollrath, D., Reversal of mutant myocilin non-secretion and cell killing: implications for glaucoma. *Hum Mol Genet* **2004,** *13* (11), 1193-204.

7. Zeng, L. C.; Han, Z. G.; Ma, W. J., Elucidation of subfamily segregation and intramolecular coevolution of the olfactomedin-like proteins by comprehensive phylogenetic analysis and gene expression pattern assessment. *FEBS Lett* **2005,** *579* (25), 5443-53.

8. Feinberg, K.; Eshed-Eisenbach, Y.; Frechter, S.; Amor, V.; Salomon, D.; Sabanay, H.; Dupree, J. L.; Grumet, M.; Brophy, P. J.; Shrager, P.; Peles, E., A glial signal consisting of gliomedin and NrCAM clusters axonal Na+ channels during the formation of nodes of Ranvier. *Neuron* **2010,** *65* (4), 490-502.

9. Eshed, Y.; Feinberg, K.; Poliak, S.; Sabanay, H.; Sarig-Nadir, O.; Spiegel, I.; Bermingham, J. R., Jr.; Peles, E., Gliomedin mediates Schwann cell-axon interaction and the molecular assembly of the nodes of Ranvier. *Neuron* **2005,** *47* (2), 215-29.

10. Eshed, Y.; Feinberg, K.; Carey, D. J.; Peles, E., Secreted gliomedin is a perinodal matrix component of peripheral nerves. *J Cell Biol* **2007,** *177* (3), 551-62.

11. Maertens, B.; Hopkins, D.; Franzke, C. W.; Keene, D. R.; Bruckner-Tuderman, L.; Greenspan, D. S.; Koch, M., Cleavage and oligomerization of gliomedin, a

transmembrane collagen required for node of ranvier formation. *J Biol Chem* **2007,** *282* (14), 10647-59.

12. Labasque, M.; Devaux, J. J.; Leveque, C.; Faivre-Sarrailh, C., Fibronectin type III-like domains of neurofascin-186 protein mediate gliomedin binding and its clustering at the developing nodes of Ranvier. *J Biol Chem* **2011,** *286* (49), 42426-34.

13. Lustig, M.; Zanazzi, G.; Sakurai, T.; Blanco, C.; Levinson, S. R.; Lambert, S.; Grumet, M.; Salzer, J. L., Nr-CAM and neurofascin interactions regulate ankyrin G and sodium channel clustering at the node of ranvier. *Current Biology* **2001,** *11* (23), 1864-1869.

14. Amor, V.; Feinberg, K.; Eshed-Eisenbach, Y.; Vainshtein, A.; Frechter, S.; Grumet, M.; Rosenbluth, J.; Peles, E., Long-term maintenance of Na+ channels at nodes of Ranvier depends on glial contact mediated by gliomedin and NrCAM. *J Neurosci* **2014,** *34* (15), 5089-98.

15. Donegan, R. K.; Hill, S. E.; Freeman, D. M.; Nguyen, E.; Orwig, S. D.; Turnage, K. C.; Lieberman, R. L., Structural basis for misfolding in myocilin-associated glaucoma. *Hum Mol Genet* **2015,** *24* (8), 2111-24.

16. Hill, S. E.; Donegan, R. K.; Nguyen, E.; Desai, T. M.; Lieberman, R. L., Molecular Details of Olfactomedin Domains Provide Pathway to Structure-Function Studies. *PLoS One* **2015,** *10* (6), e0130888.

17. Fulop, V.; Jones, D. T., Beta propellers: structural rigidity and functional diversity. *Current Opinion in Structural Biology* **1999,** *9* (6), 715-721.

18. Chen, C. K.; Chan, N. L.; Wang, A. H., The many blades of the beta-propeller proteins: conserved but versatile. *Trends Biochem Sci* **2011,** *36* (10), 553-61.

19. Donegan, R. K.; Hill, S. E.; Turnage, K. C.; Orwig, S. D.; Lieberman, R. L., The glaucoma-associated olfactomedin domain of myocilin is a novel calcium binding protein. *J Biol Chem* **2012,** *287* (52), 43370-7.

20. Witarto, A. B.; Sode, K., Increasing the hydrophobic interaction between terminal W-motifs enhances the stability of *Salmonella typhimurium* sialidase. A general strategy for the stabilization of B-propeller protein fold. *Protein Engineering* **2001,** *14* (11), 891-896.

21. Kennan, A. M.; Mansergh, F. C.; Fingert, J. H.; Clark, T.; Ayuso, C.; Kenna, P. F.; Humphries, P.; Farrar, G. J., A novel Asp380Ala mutation in the GLC1A/myocilin gene in a family with juvenile onset primary open angle glaucoma. *J Med Genet* **1998,** *35*, 957-960.

22. Stothert, A. R.; Fontaine, S. N.; Sabbagh, J. J.; Dickey, C. A., Targeting the ER-autophagy system in the trabecular meshwork to treat glaucoma. *Exp Eye Res* **2016,** *144*, 38-45.

23. Joe, M. K.; Sohn, S.; Hur, W.; Moon, Y.; Choi, Y. R.; Kee, C., Accumulation of mutant myocilins in ER leads to ER stress and potential cytotoxicity in human trabecular meshwork cells. *Biochem Biophys Res Commun* **2003,** *312* (3), 592-600.

24. Suntharalingam, A.; Abisambra, J. F.; O'Leary, J. C., 3rd; Koren, J., 3rd; Zhang, B.; Joe, M. K.; Blair, L. J.; Hill, S. E.; Jinwal, U. K.; Cockman, M.; Duerfeldt, A. S.; Tomarev, S.; Blagg, B. S.; Lieberman, R. L.; Dickey, C. A., Glucose-regulated protein 94 triage of mutant myocilin through endoplasmic reticulum-associated degradation subverts a more efficient autophagic clearance mechanism. *J Biol Chem* **2012,** *287* (48), 40661-9.

25. Burns, J. N.; Orwig, S. D.; Harris, J. L.; Watkins, J. D.; Vollrath, D.; Lieberman, R. L., Rescue of glaucoma-causing mutant myocilin thermal stability by chemical chaperones. *ACS Chemical Biology* **2010,** *5* (5), 477-487.

26. Otwinowski, Z.; Minor, W., Processing of X-ray Diffraction Data Collected in Oscillation Mode. In *Methods in Enzymology*, C.W. Carter, Jr. & R. M. Sweet, Academic Press: New York, 1997; Vol. 276, pp 307-326.

27. McCoy, A. J.; Grosse-Kunstleve, R. W.; Adams, P. D.; Winn, M. D.; Storoni, L. C.; Read, R. J., Phaser crystallographic software. *J Appl Crystallogr* **2007,** *40* (Pt 4), 658-674.

28. Adams, P. D.; Afonine, P. V.; Bunkoczi, G.; Chen, V. B.; Davis, I. W.; Echols, N.; Headd, J. J.; Hung, L. W.; Kapral, G. J.; Grosse-Kunstleve, R. W.; McCoy, A. J.; Moriarty, N. W.; Oeffner, R.; Read, R. J.; Richardson, D. C.; Richardson, J. S.; Terwilliger, T. C.; Zwart, P. H., PHENIX: a comprehensive Python-based system for macromolecular structure solution. *Acta Crystallogr D Biol Crystallogr* **2010,** *66* (Pt 2), 213-21.

29. Emsley, P.; Lohkamp, B.; Scott, W. G.; Cowtan, K., Features and development of Coot. *Acta Crystallogr D Biol Crystallogr* **2010,** *66* (Pt 4), 486-501.

30. Afonine, P. V.; Grosse-Kunstleve, R. W.; Echols, N.; Headd, J. J.; Moriarty, N. W.; Mustyakimov, M.; Terwilliger, T. C.; Urzhumtsev, A.; Zwart, P. H.; Adams, P. D., Towards automated crystallographic structure refinement with phenix.refine. *Acta Crystallogr D Biol Crystallogr* **2012,** *68* (Pt 4), 352-67.

31. Hill, S. E.; Donegan, R. K.; Lieberman, R. L., The glaucoma-associated olfactomedin domain of myocilin forms polymorphic fibrils that are constrained by partial unfolding and peptide sequence. *J Mol Biol* **2014,** *426* (4), 921-35.

32. Maurer, P.; Hohenester, E., Structural and functional aspects of calcium binding in extracellular matrix proteins. *Matrix Biology* **1997,** *15* (8-9), 569-580.

VITA

MICHELLE S. KWON

KWON was born in Kennesaw, Georgia. She attended public schools in Kennesaw, Georgia, received a B.S. in Biochemistry from Georgia Institute of Technology, Atlanta, Georgia in 2017. When she is not working on her research, Ms. Kwon enjoys attending operas and ballets, watching movies, and relaxing with her family and pets.